Single axis pointing for underactuated spacecraft with a residual angular momentum

Single Axis Pointing for Underactuated Spacecraft with a Residual Angular Momentum

G. Avanzini*[,a], Alessandro Zavoli[b], Guido De Matteis[b], Fabrizio Giulietti[c]

[a] *Department of Engineering for Innovation (DII), Universit del Salento, Ecotekne Campus, Via per Monteroni, 73100 Lecce, Italy*
[b] *Department of Machanical and Aerospace Engineering (DIMA), "Sapienza" Universit di Roma, Via Eudossiana 18, 00184 Roma, Italy*
[c] *Department of Industrial Engineering (DIN), Università di Bologna (Forlì Campus), Via Fontanelle 40, Forlì, 47121, Italy*

Abstract

The problem of aiming a generic body-fixed axis along an inertially fixed direction is dealt with for an underactuated spacecraft, in the presence of a non–zero residual angular momentum, considering a situation where only two reaction wheels (RWs) can exchange angular momentum with the spacecraft platform. The admissible pointing directions are investigated first, providing (i) an analytical condition for the feasibility of the desired pointing and (ii) a closed-form solution for the determination of the corresponding attitude with zero platform angular rate, if feasible. A nonlinear controller is then developed in the framework of singular perturbation theory, enforcing a two-timescale response to the system. Convergence to the desired attitude from arbitrary initial conditions is investigated for both rest-to-rest maneuvers and randomly generated initial tumbling conditions. Simulations are performed for a configuration representative of a small-size satellite, proving that the pointing problem can be effectively tackled even though a non–zero residual angular momentum is present, if the desired pointing direction falls within the admissible limits.

Key words: Attitude control, Underactuated spacecraft, Single-axis pointing

*Corresponding author.
Email address: giulio.avanzini@unisalento.it (G. Avanzini)

1. Introduction

Advances in spacecraft and satellite control systems succeeded in solving several challenging problems concerning attitude tracking, robust control, optimal slew maneuvers, or precision pointing [1], while assuming a number of actuators equal to, or larger than, the rotational degrees of freedom of the system, where the actuators may in some cases exploit different physical principles [2]. In the attempt of extending operational lifetime or increasing mission resilience to system failures, attitude stabilization problems in case of actuator failures have being gaining an increasing attention in the recent past. The problem is particularly relevant for small-size satellite platforms, for which a combination of weight, volume and/or budget constraint may result into the adoption of a non-redundant architecture for the attitude control system, possibly based on low-cost hardware, which further jeopardizes overall system reliability.

In this framework, the present paper explores the feasibility of a single-axis pointing maneuver for an underactuated spacecraft in the presence of a non-zero residual angular momentum vector. In this scenario, a body-fixed axis $\hat{\boldsymbol{\sigma}}$, such as the line-of-sight of a sensor, a nozzle for orbit control or an antenna, needs to be aligned to a target direction $\hat{\boldsymbol{\tau}}$, fixed in the inertial reference frame. Only two RWs are available for managing the residual angular momentum, which is a situation representative of a failure condition of a non-redundant control system or of a critical condition after multiple failures of a reaction wheel cluster. A similar problem was dealt with in a previous paper [3], where a single-axis pointing maneuver for a tri-inertial spacecraft is studied under the hypothesis of zero total angular momentum,

implementing the kinematic planning techniques developed in [4] and [5] at a dynamic level.

The hypothesis of zero residual angular momentum is common to many papers dealing with spacecraft attitude control in underactuated conditions [6]. Unfortunately, such a situation is seldom encountered in practice, for several reasons. A (possibly large) angular momentum normal to the orbit plane may be present for passive gyroscopic stabilization [7], or a (usually small) non-zero angular momentum may result from the action of environmental torques [8]. The unwanted angular momentum can be dumped by means of a torque generated by thrusters or magnetorquers for desaturating reaction and momentum wheels. However, a residual angular momentum is often present not only during standard operations, before wheel desaturation, but also at the end of the desaturation maneuver, provided that the control system, based on a switching (on-off) control logic, cannot drive the spacecraft angular momentum exactly to zero. This residual angular momentum can be large when a Y-dot control law with magnetorquers is adopted for spacecraft detumbling [9]. Its presence thus represents a realistic situation to be dealt with in practice, which makes the pointing maneuver more challenging with respect to the case when a zero overall angular momentum is assumed.

A (possibly large) angular momentum normal to the orbit plane may be present for passive gyroscopic stabilization [7], or a (usually small) non-zero angular momentum may result from the action of environmental torques [8]. The unwanted angular momentum can be dumped by means of a torque generated by thrusters or magnetorquers for desaturating reaction and mo-

mentum wheels. However, a residual angular momentum is often present not only during standard operations, before wheel desaturation, but also at the end of the desaturation maneuver, provided that the control system, based on a switching (on-off) control logic, cannot drive the spacecraft angular momentum exactly to zero. This residual angular momentum can be large when a Y-dot control law with magnetorquers is adopted for spacecraft detumbling [9]. Its presence thus represents a realistic situation to be dealt with in practice, which makes the pointing maneuver more challenging with respect to the case when a zero overall angular momentum is assumed.

A review of methods for attitude control of underactuated spacecraft is presented by Tsiotras [10]. Several studies dealt with this class of problems, considering diverse types of control hardware (thruster [11], RWs [12], control moment gyros (CMG's) [13]), for either axis-symmetric [14] or tri-inertial [6] spacecraft, in different mission scenarios (full attitude stabilization, single-axis pointing, acquisition of a desired spin state, etc.). More recently, some papers addressed the problem of attitude control of an underactuated spacecraft in the presence of a residual angular momentum.

A nonlinear control law based on the state-dependent Riccati equation is proposed in [15], which stabilizes roll and pitch angles only at a desired value, by means of two reaction wheels. A linear time-varying model predictive control law is presented in [16], with the objective of driving the underactuated spacecraft towards a prescribed attitude in the presence of a gravity gradient torque. In such a case, the angular momentum is not exactly zero, although it remains very small. Convergence to the desired attitude requires time intervals in the order of one hour and a residual error is present, with persis-

tent oscillations, which cannot be compensated by the underactuated control hardware. A control law based on a sliding mode approach for attitude control around the torqueless direction is discussed in [17], where a cluster of two single-gimbal control moment gyroscopes (SGCMG) with parallel gimbals axes is the underactuated attitude effector. The final attitude can be asymptotically attained only if the (inertially constant) angular momentum vector lies within the SGCMG cluster momentum envelope. This, in turn, requires that the direction of the gimbal axes is exactly normal to the conserved angular momentum when the desired attitude is attained, thus limiting the set of feasible attitudes to a subspace of SO(3). For any other final attitude the control law causes a permanent rotation in the neighbourhood of the prescribed attitude, with pointing errors which may be significant.

To the best of authors' knowledge, the control law discussed in the present paper is the first solution for the problem of exact pointing of a generic body–fixed axis by means of an underactuated spacecraft in the presence of a residual angular momentum. In this framework, the work extends and generalizes the results proposed by Yoon [18] and Kwon [19], where the problem was solved for pointing a principal axis of inertia along an arbitrary direction.

As a first contribution, a feasibility condition for the desired pointing maneuver is analytically determined for a generic body-fixed axis $\hat{\boldsymbol{\sigma}}$, highlighting that, when $\hat{\boldsymbol{\sigma}}$ is not a principal axis of inertia, it cannot be aligned along some inertial directions $\hat{\boldsymbol{\tau}}$, while keeping the spacecraft at rest. This latter condition requires that the body-fixed plane identified by the spin axes of the two active RWs contains the (inertially fixed) direction of the angular momentum vector. Under this constraint, the direction $\hat{\boldsymbol{\tau}}$ may become

unattainable by $\hat{\boldsymbol{\sigma}}$ and an inequality represents the feasibility condition in simple mathematical terms

The attitude that allows to maintain the body axis along the desired direction with the spacecraft platform at rest is analytically determined if spacecraft attitude is described in terms of Euler angles for the 3-1-3 elementary rotation sequence (precession, nutation and spin angles). Although affected by a singularity issue, Euler angles provide a clear and intuitive physical interpretation of the results: when spacecraft angular rate is zero, nutation angle must be $\pi/2$, whereas the final value of the spin angle indicates the distribution of angular momentum between the wheels, when the spacecraft is at rest. The pointing feasibility condition and the attitude for obtaining zero platform angular rate are shown to be independent of the magnitude of the angular momentum, provided that such a magnitude is compatible with active RW saturation levels.

After deriving a linearized system dynamics in the neighborhood of the desired attitude, controllability of the system is proven, in order to demonstrate that the problem of enforcing closed-loop stability is well-posed, at least locally, in spite of the underactuated condition of the spacecraft. Then, an almost-globally stabilizing control law is developed, which is based on a nested architecture, where the inner loop controls precession and nutation angles, and the outer loop provides convergence towards the desired value of spin angle. Singular perturbation theory is applied for both inner and outer loops in order to demonstrate convergence towards the commanded attitude when a two-timescale behavior is enforced to the system [20] by means of a proper selection of control law parameters.

More in detail, at the inner level, the fast dynamics is represented by RW response to an angular momentum command, whereas the slow dynamics is represented by the commanded nutation and precession angle rates, which determine the angular momentum command for the wheels. The resulting closed-loop system tracks the commanded values of nutation and precession angles and it represents the fast dynamics for the outer loop, where the slow dynamics is given by the prescribed spin rate. The spin rate command is implemented by enforcing a correction to the desired nutation angle, exploiting the residual angular momentum for obtaining a rotation rate around the axis along which an attitude effector is not available. When the pointing maneuver is feasible, the resulting command law for the two active RWs drives the body-fixed direction $\hat{\boldsymbol{\sigma}}$ towards $\hat{\boldsymbol{\tau}}$, so that the pointing error (that is, the angle between the unit vectors $\hat{\boldsymbol{\sigma}}$ and $\hat{\boldsymbol{\tau}}$) asymptotically approaches zero. This is proven up to the bounds of the region of admissible pointing directions.

In the next section, after a short review of spacecraft dynamics in underactuated conditions, the attitude parameters which enforce the desired pointing at zero angular rate are derived, together with the analytical condition for maneuver feasibility. After assessing system controllability at least in the neighborhood of the attitude implementing the desired pointing condition, the control strategy based on singular perturbation theory is derived in Section 3. Resulting performance of the control laws in resto-to-rest maneuvers as well as starting from arbitrary, randomly generated, initial conditions is analyzed in Section 4. A section of concluding remarks ends the paper.

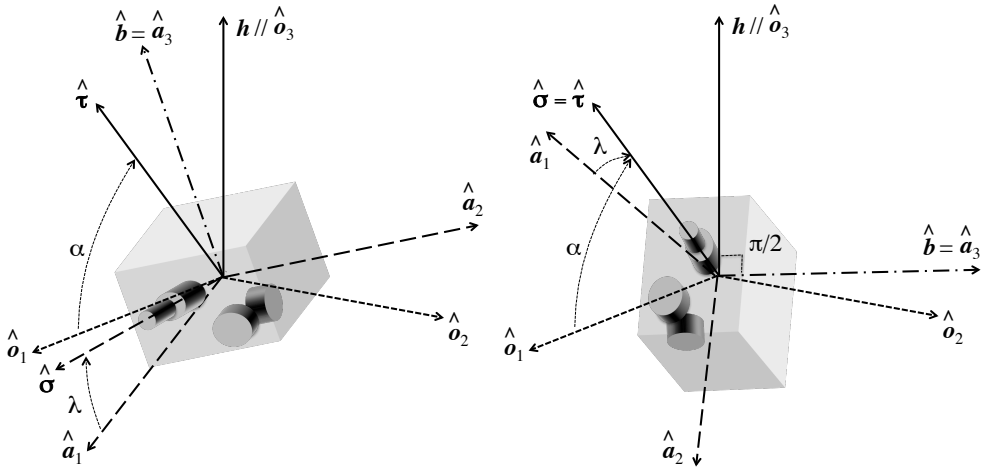

(a) initial condition (b) admissible pointing

Figure 1: Geometry of the problem.

2. Problem Statement and Mathematical Model

2.1. Spacecraft dynamics

A rigid satellite platform equipped with three identical RWs is considered, with the spin axes of the wheels aligned with the principal axes of inertia. When one of the wheels fails, it cannot provide one of the components of the control torque, resulting in an underactuated condition. Let $\mathcal{F}_B = \{G; \hat{\boldsymbol{e}}_1, \hat{\boldsymbol{e}}_2, \hat{\boldsymbol{e}}_3\}$ be a body-fixed reference frame, centered in the spacecraft center of mass, G, with axes aligned to the principal axes of inertia of the spacecraft. Without loss of generality, the spin axis of the failed wheel, $\hat{\boldsymbol{b}}$, is assumed parallel to the third axis of the body frame ($\hat{\boldsymbol{b}} \equiv \hat{\boldsymbol{e}}_3$). Thus, the spin axes of RWs available for control are parallel to $\hat{\boldsymbol{e}}_1$ and $\hat{\boldsymbol{e}}_2$, respectively.

It is also assumed that no external torque is present, so that the non-zero angular momentum vector is constant in the inertial frame. As a further

hypothesis, the magnitude of the angular momentum is assumed to be less than the momentum storage capacity of one single active wheel. This is a mild assumption, provided that, if this condition is violated, it would not be possible to drive the spacecraft angular rate to zero. In this respect, one can assume that a desaturation maneuver (performed by means of some actuators which deliver an external torque, such as magnetic actuators) already reduced the overall angular momentum below an acceptable threshold for operating the spacecraft. Under these assumptions, and expressing all vector quantities in terms of components in the body-fixed set of principal axes of inertia, spacecraft dynamics is represented as

$$\dot{\boldsymbol{H}} + \boldsymbol{\omega}^{\times}\boldsymbol{H} = \boldsymbol{0} \tag{1}$$

where $\boldsymbol{H} = \boldsymbol{J}\boldsymbol{\omega} + \boldsymbol{h}$ is the total angular momentum vector, whose magnitude $H_0 = \|\boldsymbol{H}\|$ is constant, $\boldsymbol{\omega} = (\omega_1, \omega_2, \omega_3)^T$ is the absolute angular velocity vector, $\boldsymbol{J} = \mathrm{diag}(J_1, J_2, J_3)$ is the inertia tensor (including RWs at rest), $\boldsymbol{h} = (h_1,\, h_2, 0)^T$ is the relative angular momentum of the RWs, under the assumption of a failed wheel aligned with $\hat{\boldsymbol{e}}_3$, and $\boldsymbol{v}^{\times}$ indicates the skew-symmetric matrix equivalent for the cross-product operation of vector $\boldsymbol{v} = (v_1, v_2, v_3)^T$, such that $\boldsymbol{v}^{\times}\boldsymbol{u} = \boldsymbol{v} \times \boldsymbol{u}$.

The relative angular momentum of the i–th active RW, $i = 1, 2$, is equal to $h_i = J_w\Omega_i$, where Ω_i is the wheel spin rate relative to $\mathcal{F}_B$, whereas the absolute angular momentum for the same wheel is given by $h_i^{(a)} = J_w(\Omega_i + \omega_i) = h_i + J_w\omega_i$. The dynamics of the i-th wheel, under the control of the electrical motor torque $g_{em,i}$, is thus given by

$$\dot{h}_i^{(a)} = \dot{h}_i + J_w\dot{\omega}_i = \; g_{em,i} \qquad i = 1, 2 \tag{2}$$

A two–dimensional vector $\boldsymbol{u} = (u_1, u_2)^T$ of available virtual control torques, $u_i = -\dot{h}_i = -\left(g_{em,i} - J_w\dot{\omega}_i\right)$, is introduced to attain a more compact notation. As a result, the mathematical model of spacecraft dynamics with two active RWs takes the form

$$\dot{\boldsymbol{\omega}} = \boldsymbol{J}^{-1}\left[\boldsymbol{S}\boldsymbol{u} - \boldsymbol{\omega}^{\times}\left(\boldsymbol{J}\boldsymbol{\omega} + \boldsymbol{h}\right)\right] \tag{3}$$

$$\dot{\boldsymbol{h}} = -\boldsymbol{S}\boldsymbol{u} \tag{4}$$

where

$$\boldsymbol{S}^T = \begin{bmatrix} 1 & 0 & 0 \\ 0 & 1 & 0 \end{bmatrix}$$

2.2. Kinematics

The single-axis pointing problem requires that the spacecraft attains a final attitude, where a body-fixed axis, identified by the unit vector $\hat{\boldsymbol{\sigma}}$, is aligned to a prescribed inertially-fixed direction $\hat{\boldsymbol{\tau}}$, with zero final angular speed. Without loss of generality, an inertially fixed reference frame $\mathcal{F}_I = \{G; \hat{\boldsymbol{o}}_1, \hat{\boldsymbol{o}}_2, \hat{\boldsymbol{o}}_3\}$ is introduced, such that the total angular momentum of the spacecraft $\boldsymbol{H}$ is aligned with $\hat{\boldsymbol{o}}_3$, and the axis $\hat{\boldsymbol{\tau}}$ lies in the $\hat{\boldsymbol{o}}_1$-$\hat{\boldsymbol{o}}_3$ plane, whereas $\hat{\boldsymbol{o}}_2 = \hat{\boldsymbol{o}}_3 \times \hat{\boldsymbol{o}}_1$ completes a right-handed triad. One thus has

$$\hat{\boldsymbol{o}}_1 = \hat{\boldsymbol{o}}_2 \times \hat{\boldsymbol{o}}_3 \;;\quad \hat{\boldsymbol{o}}_2 = (\boldsymbol{H} \times \hat{\boldsymbol{\tau}})/\|\boldsymbol{H} \times \hat{\boldsymbol{\tau}}\| \;;\quad \hat{\boldsymbol{o}}_3 = \boldsymbol{H}/\|\boldsymbol{H}\| \tag{5}$$

Note that the unit vector $\hat{\boldsymbol{o}}_1$ is parallel to the direction of the projection of $\hat{\boldsymbol{\tau}}$ on the plane perpendicular to $\boldsymbol{H}$. In the particular case when $\hat{\boldsymbol{\tau}}$ is parallel to $\boldsymbol{H}$, $\hat{\boldsymbol{o}}_1$ and $\hat{\boldsymbol{o}}_2$ can be selected arbitrarily on the plane perpendicular to $\hat{\boldsymbol{o}}_3$, to complete an orthogonal right-handed triad $\mathcal{F}_I$.

Spacecraft attitude with respect to $\mathcal{F}_I$ can be represented by means of a 3-1-3 sequence of precession (Ψ), nutation (Θ), and spin (Φ) Euler angles [7],

where $\Psi \in [-\pi, \pi]$, $\Theta \in [0, \pi]$, and $\Phi \in [-\pi, \pi]$. Euler angle rates are given by

$$\begin{pmatrix} \dot{\Psi} \\ \dot{\Theta} \\ \dot{\Phi} \end{pmatrix} = \begin{bmatrix} \sin\Phi/\sin\Theta & \cos\Phi/\sin\Theta & 0 \\ \cos\Phi & -\sin\Phi & 0 \\ -\sin\Phi/\tan\Theta & -\cos\Phi/\tan\Theta & 1 \end{bmatrix} \begin{pmatrix} \omega_1 \\ \omega_2 \\ \omega_3 \end{pmatrix} \tag{6}$$

whereas the expression of the coordinate transformation matrix $\mathbb{T}_{BI}$ as a function of Ψ, Θ, and Φ can be found in [21], and it is not reported here for the sake of conciseness. This attitude representation is known to be singular for $\Theta = 0, \pi$. Nonetheless, this parametrization simplifies the determination of spacecraft attitude, which corresponds to the desired pointing at zero angular rate, as outlined in the next subsection, where it will also be shown that admissible pointing attitudes require $\Theta \neq 0, \pi$. Consequently, singularity of the desired attitude in not an issue in the present analysis.

The simulation model features attitude propagation in terms of unit quaternions for avoiding issues with the singularity in the attitude representation by means of Euler angles during simulations. Current values of Euler angles are thus derived from the elements $t_{i,j}$ of the coordinate transformation matrix $\mathbb{T}_{BI}(\boldsymbol{q}_0, \bar{q}) = (\bar{q}^2 - \boldsymbol{q}^T\boldsymbol{q})\mathbb{I}_3 + 2\boldsymbol{q}\boldsymbol{q}^T - 2\bar{q}\tilde{\boldsymbol{Q}}$, where $\mathbb{I}_3$ is the 3×3 identity matrix and $\tilde{\boldsymbol{Q}}$ is the skew symmetrix matrix equivalent of the cross product, such that $\tilde{\boldsymbol{Q}}\boldsymbol{v} = \boldsymbol{q} \times \boldsymbol{v}$. In this framework one has that

$$\Psi = \text{atan2}(t_{3,1}, -t_{3,2}) \ , \quad \Theta = \text{acos}(t_{3,3}) \ , \quad \Phi = \text{atan2}(t_{1,3}, t_{2,3})$$

where $\text{atan2}(y, x)$ is the four-quadrant inverse tangent function.

2.3. Feasibility and solution of the pointing problem

When a spacecraft with only two active RWs is considered, the constraint of constant non-zero angular momentum restricts the set of admissible attitudes at rest to a compact subset of SO(3), provided that the total angular momentum of the whole satellite must lie in the plane identified by the spin axes of the active RWs (plane $\hat{\boldsymbol{e}}_1$–$\hat{\boldsymbol{e}}_2$, under the assumptions outlined above for the spacecraft model). Given the definition of body and inertial reference frames $\mathcal{F}_B$ and $\mathcal{F}_I$, respectively, the target direction $\hat{\boldsymbol{\tau}}$ can be expressed in $\mathcal{F}_I$ as $\hat{\boldsymbol{\tau}}_I = (\cos\alpha, 0, \sin\alpha)^T$ where $\alpha \in [-\pi/2, \pi/2]$ is the elevation of $\hat{\boldsymbol{\tau}}$ over the $\hat{\boldsymbol{o}}_1$-$\hat{\boldsymbol{o}}_2$ plane. On the other hand, the unit vector $\hat{\boldsymbol{\sigma}}$ can be parametrized in $\mathcal{F}_B$ as $\hat{\boldsymbol{\sigma}} = (\cos\lambda\cos\eta, \cos\lambda\sin\eta, \sin\lambda)^T$ where λ is the elevation over the $\hat{\boldsymbol{e}}_1$–$\hat{\boldsymbol{e}}_2$ plane, and η is the azimuth with respect to $\hat{\boldsymbol{e}}_1$. Provided that the frame $\mathcal{F}_B$ can always be chosen such that $\hat{\boldsymbol{e}}_3^T\hat{\boldsymbol{\sigma}} \geq 0$, the analysis is restricted to the case $\lambda \in [0, \pi/2]$ without loss of generality.

In order to simplify the derivation of the target attitude, an auxiliary body-fixed reference frame $\mathcal{F}_A = \{G; \hat{\boldsymbol{a}}_1, \hat{\boldsymbol{a}}_2, \hat{\boldsymbol{a}}_3\}$ is introduced, which is obtained rotating $\mathcal{F}_B$ by an angle η about the axis $\hat{\boldsymbol{e}}_3$, that is, $\mathbb{T}_{AB} = \mathbb{R}_3(\eta)$. As a consequence, the auxiliary reference frame can be parametrized by means of a 3-1-3 set of Euler-angles, $\{\Psi', \Theta', \Phi'\}$, such that $\Phi' = \Phi + \eta$, $\Theta' = \Theta$, and $\Psi' = \Psi$. The unit vector $\hat{\boldsymbol{\sigma}}$ belongs to the plane $\hat{\boldsymbol{a}}_1$-$\hat{\boldsymbol{a}}_3$ of $\mathcal{F}_A$, so that its components are given by

$$\hat{\boldsymbol{\sigma}}_A = (\cos\lambda, 0, \sin\lambda)^T \tag{7}$$

The derivation of a maneuver feasibility condition, with the determination of an attitude which guarantees the prescribed alignment of $\hat{\boldsymbol{\sigma}}$ and $\hat{\boldsymbol{\tau}}$ with zero

residual angular rate is performed describing spacecraft attitude in terms of the angular position of this auxiliary reference frame.

Starting from an arbitrary initial attitude, identified by the angles Ψ_i, Θ_i, and Φ_i, the final attitude represented by Ψ_f, Θ_f, and Φ_f must satisfy two constraints, namely

1. the spacecraft is at rest, that is, $\boldsymbol{\omega} = 0$;
2. $\hat{\boldsymbol{\sigma}}$ is aligned with $\hat{\boldsymbol{\tau}}$, that is, $\hat{\boldsymbol{\sigma}} = \hat{\boldsymbol{\tau}}$.

The first condition requires that, at the end of the maneuver, the total angular momentum is completely stored in the RWs, that is, $\boldsymbol{H}$ must lie on the $\hat{\boldsymbol{a}}_1$-$\hat{\boldsymbol{a}}_2$ plane, which implies $\hat{\boldsymbol{a}_3}^T \boldsymbol{H} = 0$. Remembering that total angular momentum is parallel to $\hat{\boldsymbol{o}}_3$, so that $\boldsymbol{H}_I = (0, 0, H_0)^T$, and $\boldsymbol{H} = \mathbb{T}_{BI} \boldsymbol{H}_I$, this condition can be expressed as $h_3 = H_0 \cos\Theta = 0$. Thus, the first requirement is met if $\cos\Theta_f = 0$, that is, the nutation angle at the end of the pointing maneuver is $\Theta_f = \pi/2$. This implies that admissible final attitudes with zero angular rate are never singular. At the end of the pointing maneuver, when $\Theta = \Theta_f$, the coordinate transformation matrix achieves the form

$$\mathbb{T}_{AI}(\Psi_f, \Phi_f) = \begin{bmatrix} \cos\Phi_f \cos\Psi_f & \cos\Phi_f \sin\Psi_f & \sin\Phi_f \\ -\sin\Phi_f \cos\Psi_f & -\sin\Phi_f \sin\Psi_f & \cos\Phi_f \\ \sin\Psi_f & -\cos\Psi_f & 0 \end{bmatrix} \tag{8}$$

The second requirement (alignment of axis $\hat{\boldsymbol{\sigma}}$ with $\hat{\boldsymbol{\tau}}$) is thus enforced by equating the components of $\hat{\boldsymbol{\sigma}}$ and $\hat{\boldsymbol{\tau}} = \mathbb{T}_{AI} \hat{\boldsymbol{\tau}}_I$, when both vectors are

expressed in $\mathcal{F}_A$, that is,

$$\begin{pmatrix} \cos\lambda \\ 0 \\ \sin\lambda \end{pmatrix} = \begin{pmatrix} \cos\Phi_f \cos\Psi_f \cos\alpha + \sin\Phi_f \sin\alpha \\ -\sin\Phi_f \cos\Psi_f \cos\alpha + \cos\Phi_f \sin\alpha \\ \sin\Psi_f \cos\alpha \end{pmatrix} \tag{9}$$

According to Eq. (9) (third row), the precession angle Ψ_f must satisfy the condition

$$\sin\Psi_f = \sin\lambda / \cos\alpha \tag{10}$$

which admits two real solutions $\Psi_{f,1} = \Psi_f^\star$ and $\Psi_{f,2} = \pi - \Psi_f^\star$, with $\Psi_f^\star = \sin^{-1}(\sin\lambda/\cos\alpha)$ if

$$|\alpha| \leq \pi/2 - |\lambda| \tag{11}$$

The inequality in Eq. (11) represents a feasibility condition, as the pointing maneuver becomes possible only when the elevation of the axis $\hat{\boldsymbol{\tau}}$ over the plane perpendicular to the angular momentum vector $\boldsymbol{H}$ is less than the angular distance between $\hat{\boldsymbol{\sigma}}$ and $\hat{\boldsymbol{b}}$. Figure 2 shows the regions of admissible (in black) and forbidden (in gray) target directions over the unit sphere for a few values of λ.

The first and second rows of Eq. (9) form a linear system of equations in the unknowns $X = \cos\Phi_f$ and $Y = \sin\Phi_f$, which can be written as

$$\begin{cases} aX + bY &= c \\ bX - aY &= 0 \end{cases} \tag{12}$$

where $a = \cos\Psi_f \cos\alpha$, $b = \sin\alpha$, and $c = \cos\lambda \geq 0$, whose solution is $X = ac/(a^2+b^2)$, $Y = bc/(a^2+b^2)$. Therefore, Φ_f can be found by using the four-quadrant inverse tangent function, that is, $\Phi_f = \text{atan2}(b, a) =$

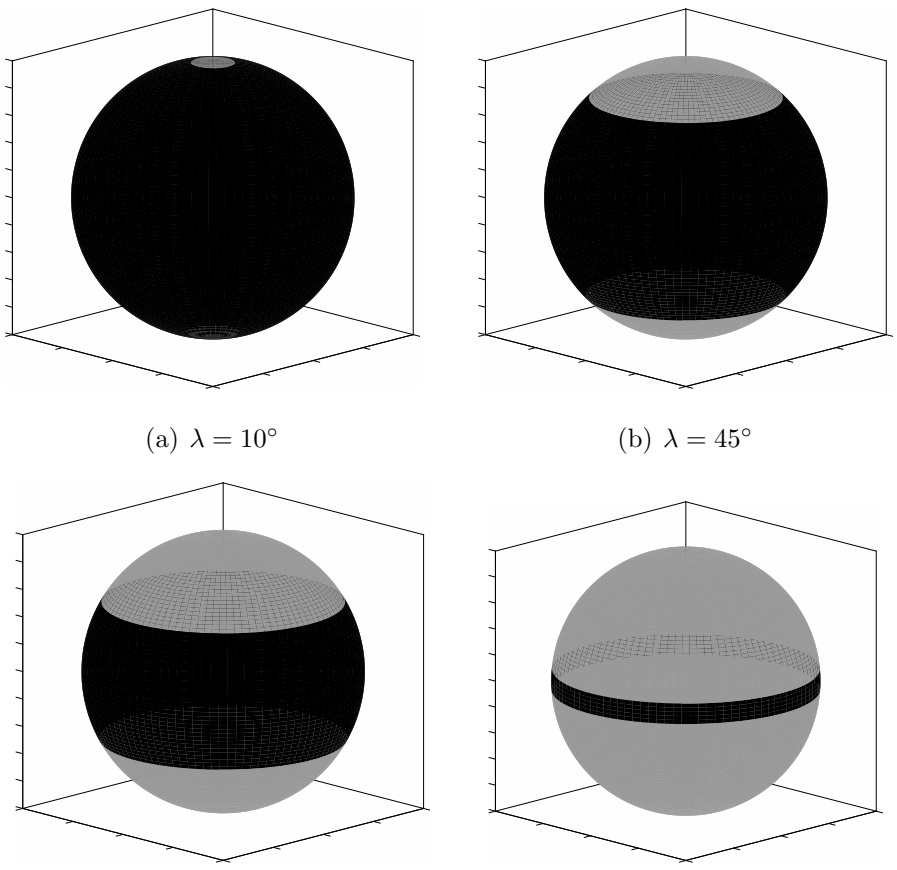

(a) $\lambda = 10°$ (b) $\lambda = 45°$

(c) $\lambda = 60°$ (d) $\lambda = 85°$

Figure 2: Admissible (black) and unaccessible (grey) target directions $\hat{\boldsymbol{\tau}}$ in $\mathcal{F}_I$ for different values of λ.

$\text{atan2}\left(\sin\alpha,\, \cos\alpha\cos\Psi_f\right)$. Two attitudes realize the single-axis pointing with spacecraft at rest, one for each solution of Eq. (10). Letting $\Phi^\star = \text{atan2}\left(\sin\alpha,\, \cos\alpha\cos\Psi^\star\right)$ and recalling the relation between Euler angles for $\mathcal{F}_B$ and $\mathcal{F}_A$ frames, it is

$$(\Psi, \Theta, \Phi)_f = \left\{\left(\Psi^\star, \pi/2, \Phi^\star - \eta\right), \left(\pi - \Psi^\star, \pi/2, \pi - \Phi^\star - \eta\right)\right\} \qquad (13)$$

2.4. Remarks

The constraint imposed by conservation of total angular momentum, $\boldsymbol{H}$, of the system formed by spacecraft platform and the active RWs provides some physical insight, useful for the derivation of a suitable control law. First of all, by expressing the equation $\boldsymbol{H} = \boldsymbol{J}\boldsymbol{\omega} + \boldsymbol{h} = \mathbb{T}_{BI}\boldsymbol{H}_I$, with $\boldsymbol{H}_I = (0, 0, H_0)^T$, in terms of body-frame components, one has that

$$\begin{pmatrix} J_1\omega_1 + h_1 \\ J_2\omega_2 + h_2 \\ J_3\omega_3 \end{pmatrix} = H_0 \begin{pmatrix} \sin\Phi\sin\Theta \\ \cos\Phi\sin\Theta \\ \cos\Theta \end{pmatrix} \tag{14}$$

The relationship between nutation angle Θ and angular velocity component along the failed axis $\hat{\boldsymbol{b}} = \hat{\boldsymbol{e}}_3$ is apparent. In particular, one has $\omega_3 = (H_0/J_3)\cos\Theta$, which clearly implies that imposing a terminal value of $\omega_3 = 0$ is equivalent to require that $\Theta_f = \pi/2$. Thus, the RWs can absorb the whole angular momentum vector, only if $\Theta = \pi/2$. This is equivalent to reducing the number of available rotational degrees of freedom to two.

It is also worthwhile to mention that, when the spacecraft is at rest, Eq. (14) states that $h_1 = H_0\sin\Phi_f$, $h_2 = H_0\cos\Phi_f$. The angle Φ_f thus defines the allocation of the total angular momentum among the two RWs, and it coincides with the desired final value of the spin angle for the auxiliary frame, $\mathcal{F}_A$. One can finally note that, when a pointing on the boundary of the feasible region is sought, such that $|\alpha| = \pi/2 - |\lambda|$, Eq. (10) implies that $\Psi_f = \pm\pi/2$, and, as a consequence, the solutions for the system in Eq. (12) are given by $\Phi_f = \pm\pi/2$. Remembering that also $\Theta_f = \pi/2$, for $\boldsymbol{\omega} = \boldsymbol{0}$, all Euler angles are equal to $\pi/2$ (in magnitude) for this limit case.

3. Controller synthesis for exact pointing

The control objective is to drive the spacecraft towards the desired admissible poiting condition from arbitrary initial conditions, while transferring the residual angular momentum to the active RWs. As a preliminary result, controllability of the system in the neighborhood of the desired pointing attitude is assessed. Then, almost global stabilization is achieved by means of a nested, inner/outer loop architecture that generates asymptotic convergence towards the desired attitude from arbitrary initial conditions.

3.1. Controllability of the linearized system

Analysis of spacecraft rotational dynamics in the neighborhood of the target attitude is performed via a linearization of the complete set of nonlinear spacecraft equations of motion, namely Eqs. (6), (3), and (4). The state vector, written in error form, is given by

$$\boldsymbol{x}^T = (e_\Psi,\ e_\Theta,\ e_\Phi,\ \boldsymbol{\omega}^T,\ \boldsymbol{e}_h{}^T)$$

where $e_\Psi = \Psi - \Psi_f$, $e_\Theta = \Theta - \pi/2$, $e_\Phi = \Phi - \Phi_f$, and $\boldsymbol{e}_h = (h_1 - h_{1,f},\ h_2 - h_{2,f})^T$. When higher-order terms are dropped, a linear time-invariant system of 8 first-order ordinary differential equations is obtained. Conservation of angular momentum allows one to drop three variables and derive a 5^{th}–order system in the form

$$\begin{pmatrix} \dot{e}_\Psi \\ \dot{\boldsymbol{\omega}} \\ \dot{e}_{h1} \end{pmatrix} = \begin{bmatrix} 0 & \boldsymbol{h}_f^T/H_0 & 0 \\ \mathbf{0} & -\boldsymbol{J}^{-1}\boldsymbol{h}_f^\times & \mathbf{0} \\ 0 & \mathbf{0^T} & 0 \end{bmatrix} \begin{pmatrix} e_\Psi \\ \boldsymbol{\omega} \\ e_{h1} \end{pmatrix} + \begin{bmatrix} \mathbf{0}^T \\ \boldsymbol{J}^{-1} \\ \boldsymbol{G} \end{bmatrix} \boldsymbol{S}\boldsymbol{u} \tag{15}$$

where $\boldsymbol{x} = (e_\Psi, \boldsymbol{\omega}^T, e_{h1})^T$ is the state vector, $\boldsymbol{u} = (u_1, u_2)^T$ is the control vector, the matrix $\boldsymbol{S}$ is defined as in subsection 2.1 and $\boldsymbol{0} = (0,0,0)^T$, $\boldsymbol{G} = (-1,0,0)$. This set of states guarantees that, when the reduced-order system reaches the origin, dropped variables also approach their desired values. In fact, if $\omega_3 \to 0$, then $\Theta \to \pi/2$; similarly, the conditions $\boldsymbol{\omega} \to 0$ and $h_1 \to h_{f1}$ imply that $h_2 \to h_{f2}$ and, as a further consequence, $\Phi \to \Phi_f$.

Controllability of the system in Eq. (15), requires full rank of the matrix $\mathcal{C} = \left[\boldsymbol{B}, \boldsymbol{AB}, \boldsymbol{A}^2\boldsymbol{B}, \boldsymbol{A}^3\boldsymbol{B}, \boldsymbol{A}^4\boldsymbol{B}\right]$, where $\boldsymbol{A}$ and $\boldsymbol{B}$ are the state and control matrices. Letting $K_s = \left(J_2 h_{f2}^2 + J_1 h_{f1}^2\right) / \left(J_1 J_2 J_3\right)$ and $K_d = (J_1 - J_2)/(H_0 J_1 J_2 J_3)$, it is

$$\mathcal{C} = \begin{bmatrix} 0 & 0 & \frac{h_{f1}}{H_0 J_1} & \frac{h_{f2}}{H_0 J_2} & 0 & 0 & K_d \frac{h_{f1} h_{f2}^2}{J_1} & -K_d \frac{h_{f1}^2 h_{f2}}{J_2} & 0 & 0 \\ \frac{1}{J_1} & 0 & 0 & 0 & -\frac{h_{f2}^2}{J_1^2 J_3} & \frac{h_{f1} h_{f2}}{J_1 J_2 J_3} & 0 & 0 & K_s \frac{h_{f2}^2}{J_1^2 J_3^2} & K_s \frac{h_{f2} h_{f1}}{J_1 J_2^2 J_3} \\ 0 & \frac{1}{J_2} & 0 & 0 & \frac{h_{f1} h_{f2}}{J_1 J_2 J_3} & -\frac{h_{f1}^2}{J_2^2 J_3} & 0 & 0 & -K_s \frac{h_{f2} h_{f1}}{J_1 J_2 J_3} & -K_s \frac{h_{f1}^2}{J_2^2 J_3} \\ 0 & 0 & -\frac{h_{f2}}{J_1 J_3} & \frac{h_{f1}}{J_2 J_3} & 0 & 0 & K_s \frac{h_{f2}}{J_1 J_3} & -K_s \frac{h_{f1}}{J_2 J_3} & 0 & 0 \\ -1 & 0 & 0 & 0 & 0 & 0 & 0 & 0 & 0 & 0 \end{bmatrix} \tag{16}$$

Sufficient condition for controllability is that all 5 rows of $\mathcal{C}$ are linearly independent, and one easily notes that all pairs of rows are linearly independent, with two relevant exceptions. First, rank of $\mathcal{C}$ drops to 2 if $h_{f1} = h_{f2} = 0$, but this condition is ruled out by the fact that $\|\boldsymbol{h}_f\| = H_0 > 0$, provided that if the total angular momentum is non–zero, at least one of the relative angular momenta of the active RWs must be non-zero in the final condition, when the spacecraft is at rest.

A second critical condition is obtained if $h_{f2} = 0$, that is, $\Phi_f = \pm\pi/2$, so that rows 2 and 5 are no longer linearly independent. This condition occurs when $\hat{\boldsymbol{\tau}}$ lies on the boundaries of the region of feasible pointing directions,

and rank loss of $\mathcal{C}$ is caused by the selection of e_{h1} as the 5-th state variable in the state vector of the reduced order model. If one considers the dual reduced-order system obtained by selecting e_{h2} instead of e_{h1}, controllability of the resulting linear time-invariant system is easily verified. Conversely, the controllability matrix for the dual system using e_{h2} as the 5^{th} state variable (not reported, for the sake of conciseness) looses rank when $\Phi_f = 0, \pi$, that is, for those pointing directions perpendicular to the direction of the residual angular momentum, namely $\alpha = 0$. However, the nonlinear system given by Eqs. (6), (3), and (4) remains first-order controllable also for $\Phi_f = \pm\pi/2$, for an appropriate choice of the 5^{th} state variable.

Once controllability is assessed, a static full-state feedback control law in the form $\boldsymbol{u} = \boldsymbol{K}\boldsymbol{x}$, which stabilizes the linearized system of Eq. (15) about the origin, can be synthesized in the framework of LQR control theory [22, 23]. This represents a robust and rigorous approach to select the optimal control gain matrix $\boldsymbol{K} \in \mathbb{R}^{2\times 5}$ that provides local asymptotic stability and optimal closed-loop performance, in a neighborhood of the equilibrium point, with the desired pointing attitude. Unfortunately, the local nature of the result makes it unsuitable for large initial errors, so that a different approach is derived in the next paragraphs.

3.2. Angular momentum command for precession and nutation control

By combining angular momentum conservation, Eq. (14), with Euler angle kinematic equations, Eq. (6), Euler angle rates can be expressed as a function of residual angular momentum components in the body frame and

angular momentum stored in the active RWs,

$$\begin{aligned}
\dot{\Psi} &= (H_0/J_1)\sin^2\Phi + (H_0/J_2)\cos^2\Phi + \\
&\quad - (h_1/J_1)(\sin\Phi/\sin\Theta) - (h_2/J_2)(\cos\Phi/\sin\Theta) \qquad (17)\\
\dot{\Theta} &= [(H_0/J_1) - (H_0/J_2)]\sin\Phi\cos\Phi\sin\Theta + \\
&\quad - (h_1/J_1)\cos\Phi + (h_2/J_2)\sin\Phi \qquad (18)\\
\dot{\Phi} &= (H_0/J_3)\cos\Theta - \dot{\Psi}\cos\Theta \qquad (19)
\end{aligned}$$

In this situation only two Euler angles can be directly controlled at the same time, by enforcing prescribed values to the relative angular momenta, h_1 and h_2, which result into desired values of precession and nutation rates, written in the form

$$\dot{\Psi}_{des} = \frac{1}{\tau_\Psi}(\Psi_f - \Psi) \ , \quad \dot{\Theta}_{des} = \frac{1}{\tau_\Theta}(\Theta_f - \Theta) \qquad (20)$$

where a first order dynamics with time constants τ_Ψ and τ_Θ is specified for the evolution of Ψ and Θ, respectively. Upon substitution of $\dot{\Psi}_{des}$ and $\dot{\Theta}_{des}$ into Eqs. (17) and (18), the resulting RW angular momenta are

$$\begin{aligned}
h_{1,des} &= H_0\sin\Phi\sin\Theta - J_1\dot{\Theta}_{des}\cos\Phi - J_1\dot{\Psi}_{des}\sin\Phi\sin\Theta \\
h_{2,des} &= H_0\cos\Phi\sin\Theta + J_2\dot{\Theta}_{des}\sin\Phi - J_2\dot{\Psi}_{des}\cos\Phi\sin\Theta
\end{aligned} \qquad (21)$$

Provided that RW dynamics can be conveniently described by means of a first-order model,

$$\dot{h}_i = \frac{1}{\tau_h}(h_{i,des} - h_i) \ , \quad i = 1,2 \qquad (22)$$

an appropriate selection of the time constants, $\tau_\Psi,\ \tau_\Theta \gg \tau_h$ in Eq. (20) enforces a two-timescale response, where RWs track the required values, $h_{1,des}$

and $h_{2,des}$, on a faster timescale than the desired evolution of precession and nutation angles.

For large initial errors, the inner system composed by Eqs. (17), (18), and Eqs. (22) is recast in standard singular perturbation form [20],

$$\dot{\boldsymbol{x}} = \boldsymbol{f}(\boldsymbol{x}, \boldsymbol{z}, t, \varepsilon) \tag{23}$$

$$\varepsilon \dot{\boldsymbol{z}} = \boldsymbol{g}(\boldsymbol{x}, \boldsymbol{z}, t, \varepsilon) \tag{24}$$

with $\boldsymbol{z} = \boldsymbol{h}$, $\boldsymbol{x} = (\Psi, \Theta)^T$, and $\varepsilon = \tau_h \ll T$ is a fast time constant, much smaller than $T = \min(\tau_\Psi, \tau_\Theta, T_\Phi)$, where $T_\Phi = 2\pi J_3/H_0$ is an estimate of the rotation period of the spin angle.

Theorem 2.1 in [20] provides three conditions under which a uniform approximation for slow and fast states is available. Let $\bar{\boldsymbol{x}}(t)$ and $\bar{\boldsymbol{z}}(t)$ represent the quasi-steady state solutions of $\boldsymbol{x}$ and $\boldsymbol{z}$, respectively, with $\bar{\boldsymbol{x}}(t)$ representing the solution of the reduced order model

$$\dot{\bar{\boldsymbol{x}}} = \boldsymbol{f}(\bar{\boldsymbol{x}}, \bar{\boldsymbol{z}}, t, 0)$$

for slow state variables, when fast states are at equilibrium, that is, $\bar{\boldsymbol{z}} = \boldsymbol{h}(\bar{\boldsymbol{x}}, t)$ is a solution for the system $\boldsymbol{g}(\bar{\boldsymbol{x}}, \bar{\boldsymbol{z}}, t, 0) = \boldsymbol{0}$. The expansion

$$\boldsymbol{x} = \bar{\boldsymbol{x}}(t) + \mathcal{O}(\varepsilon) \tag{25}$$

$$\boldsymbol{z} = \bar{\boldsymbol{z}}(t) + \hat{\boldsymbol{z}}(\tau) - \bar{\boldsymbol{z}}(t_0) + \mathcal{O}(\varepsilon) \tag{26}$$

provides a uniform approximation of the exact solution for slow, $\boldsymbol{x}(t)$, and fast states, $\boldsymbol{z}(t)$, if (i) $\boldsymbol{h}(\bar{\boldsymbol{x}}, t)$ is an isolated root of the algebraic equation $\boldsymbol{g}(\bar{\boldsymbol{x}}, \bar{\boldsymbol{z}}, t, 0) = \boldsymbol{0}$ (Assumption 1.1); (ii) $\boldsymbol{g}(\boldsymbol{x}_0, \bar{\boldsymbol{z}}, t, 0) = \boldsymbol{0}$ is asymptotically stable uniformly for any initial value of slow and fast states, $\boldsymbol{x}_0$ and $\boldsymbol{z}_0$ at

time t_0 (Assumption 2.1); and (iii) the eigenvalues of the Jacobian matrix $\partial \boldsymbol{g}/\partial \boldsymbol{z}$ are smaller than a fixed negative quantity (Assumption 2.2). The term $\hat{\boldsymbol{z}}(\tau)$ in Eq. (26) is the so called boundary layer solution of the fast dynamic system

$$\varepsilon \dot{\hat{\boldsymbol{z}}} = \boldsymbol{g}(\boldsymbol{x}_0, \hat{\boldsymbol{z}}, t, 0)$$

with $\hat{\boldsymbol{z}}(0) = \boldsymbol{z}_0$ as initial condition. The evolution of $\hat{\boldsymbol{z}}(\tau)$ represents the fast transient that drives the fast states towards their quasi-steady approximation, $\bar{\boldsymbol{z}}(t)$.

In the present application the dynamics of $\boldsymbol{x}$ and $\boldsymbol{z}$ explicitly depends on time, because of the (at this stage still uncontrolled) variation of the spin angle, Φ, ruled by Eq. (19). The fast dynamics is represented by the first-order response of the active RWs, which satisfies the aforementioned assumptions 1.1, 2.1, and 2.2. in [20], provided that (i) the equilibrium $\boldsymbol{h} = \boldsymbol{h}_{des}$ is an isolated root for the equation $\boldsymbol{h}_{des}(\Psi_0, \Theta_0, \Phi(t_0)) - \bar{\boldsymbol{h}} = 0$; (ii) this solution is clearly asymptotically stable uniformly for any initial value of slow and fast states, $\boldsymbol{x}_0$ and $\boldsymbol{z}_0$ at time t_0; and (iii) the eigenvalues of the Jacobian matrix $\partial \boldsymbol{g}/\partial \boldsymbol{z}$, $\lambda_1 = \lambda_2 = -1$ are constant, hence smaller than a prescribed negative quantity.

At this point a local theorem can be invoked for proving asymptotic stability of states towards Θ_f, Ψ_f, and $\boldsymbol{h}_f$. In particular, once the system is rewritten in terms of error variables, Theorem 11.4 of Ref. [24] provides a proof of exponential stability, under five conditions which apply to the considered system (see Appendix for details), so as to demonstrate that almost global stability is achieved under the control law that drives Ψ and Θ towards their desired values, Ψ_f and $\Theta_f = \pi/2$, with $\|\boldsymbol{\omega}\| = 0$. The only exception

is represented by singular initial attitudes, when $\Theta = 0$ or π exactly. In the unlikely event of such a situation, an initial control action on the active wheels can be implemented, in order to drive the spacecraft out of the singular attitude and allow the control to work properly from any non-singular attitude.

3.3. Control of the spin angle

The spin angle Φ is not controlled by means of the angular momentum command described above, so that Φ takes an unpredictable value $\Phi_\infty \in [-\pi, \pi]$, if Ψ and Θ converge asymptotically towards their final values, being in general $\Phi_\infty \neq \Phi_f$. A single axis rotation around $\hat{\boldsymbol{e}}_3$ would be sufficient for achieving the desired alignment, but no control torque, nor wheel angular momentum is available around that axis. Nonetheless, introducing an outer control loop, a spin rate can be generated by means of a nutation angle, which projects a component of the residual angular momentum, $H_0 \cos\Theta$, along $\hat{\boldsymbol{e}}_3$.

Letting $\dot{\Phi}_{des} = (\Phi_{des} - \Phi)/\tau_\Phi$, a perturbed value of the required nutation angle is considered, $\Theta^\star = \Theta_f + \varepsilon_\Theta$, such that for $\Theta = \Theta^\star$ the commanded spin rate is achieved, if

$$\dot{\Phi}_{des} = [(H_0/J_3) + \dot{\Psi}_{des}] \cos\Theta^\star \tag{27}$$

being from Eq. (27) $\sin\varepsilon_\Theta = \cos\Theta^\star = -\dot{\Phi}_{des}/[(H_0/J_3) + \dot{\Psi}_{des}]$. An incremented desired nutation rate in the form $\dot{\Theta}^\star_{des} = (\Theta^\star - \Theta)/\tau_\Theta$ is thus enforced, with the same precession rate command, $\dot{\Psi}_{des} = (\Psi_{des} - \Psi)/\tau_\Psi$, and wheel angular momentum command, specified for the inner loop by Eq. (21). Note that, when Φ approaches the value prescribed by the pointing condition, Φ_f,

the desired spin rate converges towards zero, hence the perturbation ε_Θ of the nutation angle with respect to its desired value also vanishes, and the spacecraft achieves a detumbled condition at the desired pointing attitude.

Stability of the complete system including the outer loop is also inferred on the basis of the singular perturbation approach, recalling again Theorem 2.1 in [20], under the hypotheses that (i) the spin angle is now the only slow state, $x = \Phi$, (ii) fast states are $\boldsymbol{z} = (\Psi, \Theta, h_1, h_2)^T$, and (iii) the perturbation parameter is now the fast timescale $\varepsilon = \tau_f = \max(\tau_\Psi, \tau_\Psi)$, that is, the slowest time constant for the linear response enforced on nutation and precession angles. A slower response is enforced on spin angle, where the slow time constant is $T_s = \tau_\Phi \gg \tau_f$.

The equilibrium $\bar{\boldsymbol{z}} = (\Psi_f, \Theta_f, h_{1f}, h_{2f})^T$ for fast states is an isolated and exponentially stable root for the system $\boldsymbol{g}(\bar{x}, \bar{\boldsymbol{z}}, t, 0) = \boldsymbol{0}$ (see above and Appendix), so that Assumptions 1.1 and 2.1 both hold. Letting $K_\Psi = \tau_f/\tau_\Psi$, $K_\Theta = \tau_f/\tau_\Theta$ (where either one between K_Ψ and K_Θ is equal to 1 and the other one is greater than 1), and $K_h = \tau_f/\tau_h \gg 1$, the dynamics enforced on the inner system by the angular momentum command derived for the inner loop is given by

$$\varepsilon\dot{\Psi} = K_\Psi(\Psi_f - \Psi) \quad ; \quad \varepsilon\dot{\Theta} = K_\Theta(\Theta^\star - \Theta)$$
$$\varepsilon\dot{h}_1 = K_h(h_{1,des} - h_1) \quad ; \quad \varepsilon\dot{h}_2 = K_h(h_{2,des} - h_2)$$

The eigenvalues $-K_\Psi$, $-K_\Theta$, and $-K_h$ of the Jacobian matrix $\partial\boldsymbol{g}/\partial\boldsymbol{z}$ are all equal or smaller than -1, so that Assumption 2.2 is also satisfied, and a uniform approximation in the form of Eqs. (25)-(26) is available.

A bound on the maximum value of $\dot{\Phi}_{des}$ needs to be introduced, for avoiding that the required angular momentum component along $\hat{\boldsymbol{e}}_3$ exceeds a pre-

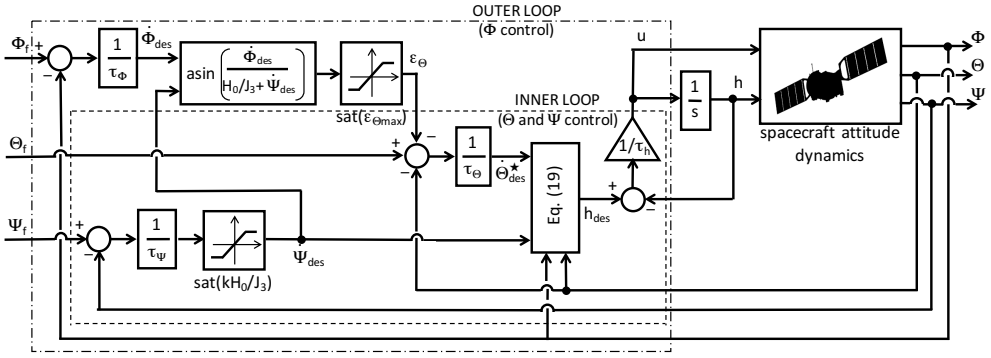

Figure 3: Architecture of the control law.

scribed percentage of H_0. This is obtained by saturating the maximum nutation angle increment ε_Θ below a prescribed threshold. Such a constraint obviously limits the maximum available spin rate, making the second step of the manoeuvre possibly slow, especially if a small residual angular momentum, H_0, is available, but this further confirms, on physical grounds, the validity of the timescale separation assumption. At the same time, a small nutation angle increment also reduces coupling with other axes. The values of H_0 and the bound on ε_Θ are thus the most relevant driving factors in determining converge speed. Finally, a bound of the desired precession rate is also required, where $\dot{\Psi}_{des} < (\dot{\Psi})_{des,\max} = kH_0/J_3)$, with $k < 1$, so that the denominator in the definition of the nutation angle increment required for spin angle control, $\sin\varepsilon_\Theta$, never vanishes. The resulting control system is schematically represented in Fig. 3, where the inner and outer loops are highlighted.

3.4. Time constants and saturation

The time constant τ_h of RW response is representative of its dynamic characteristics, so it is related to hardware type and performance. Conversely,

the time constants for required precession, nutation and spin rates, namely τ_Ψ, τ_Θ, and τ_Φ, are design parameter for the control laws, with values which can be arbitrarily higher than τ_h, thus enforcing the two-timescale behavior, upon which the control system architecture is based. Quite obviously, if time constants for desired Euler angle rates are higher, separation between timescales is wider, thus allowing for a smooth, alas slow, convergence towards the desired attitude.

If a more aggressive maneuver is to be dealt with, in order to attain faster convergence, higher Euler angle rates can be realized by choosing smaller time constants, provided that τ_Ψ, τ_Θ, and τ_Φ remain at least approximately one order of magnitude greater than τ_h. However, if initial attitude error is large, the corresponding value of desired Euler angle rates may result into high values of commanded wheel angular momenta, which in turn cause wheel torque saturation, where wheel response becomes linear with time, with a slower convergence rate of $\boldsymbol{h}$ towards $\boldsymbol{h}_{des}$. More important, timescale separation between wheel response and Euler angle variation is no longer guaranteed, hence overall spacecraft stability during the maneuver.

In these circumstances, implementation of the wheel angular momentum command requires a control on RW torque saturation. Letting $u_i = (h_{i,des} - h_i)/\tau_h$ be the desired wheel torque for the i–th active wheel, $i = 1, 2$, and g_{max} the maximum wheel motor torque, a saturation factor $f = \max(|\boldsymbol{u}|/g_{max})$ is introduced. If $f < 1$, both wheel commands are within saturation limits and the nominal implementation of the control law is adopted. If $f > 1$, saturation occurs on at least one of the wheels, and the desired wheel commands are reduced by scaling desired precession and nutation rates, $\dot{\Phi}_{des}$ and $\dot{\Theta}_{des}$,

in Eq. (21) by a factor, $k_{sat} \leq 1$, such that

$$\begin{aligned} \bar{h}_{1,des} &= H_0 \sin\Phi \sin\Theta - k_{sat}(J_1 \dot{\Theta}_{des} \cos\Phi + J_1 \dot{\Psi}_{des} \sin\Phi \sin\Theta) \\ \bar{h}_{2,des} &= H_0 \cos\Phi \sin\Theta + k_{sat}(J_2 \dot{\Theta}_{des} \sin\Phi - J_2 \dot{\Psi}_{des} \cos\Phi \sin\Theta) \end{aligned} \tag{28}$$

with

$$k_{sat} = K \left[1 - \kappa \left(1 - e^{-(f-1)^2} \right) \right] \tag{29}$$

where $0 < \kappa < 1$, and K is evaluated as follows. When the control torque which violates the saturation level most severely is u_1, an updated value of $h^{\star}_{1,des}$ is defined as

$$h^{\star}_{1,des} = h_1 + \tau_h \, g_{max} \, \mathrm{sign}(h_{1,des} - h_1)$$

The corresponding value of K is obtained by inverting the first of Eqs. (21), that is, letting

$$K = -(h^{\star}_{1,des} - H_0 \sin\Phi \sin\Theta)/(J_1 \dot{\Theta}_{des} \cos\Phi + J_1 \dot{\Psi}_{des} \sin\Phi \sin\Theta)$$

Similarly, when u_2 exceeds the saturation limit more severely, it is

$$h^{\star}_{2,des} = h_2 + \tau_h \, g_{max} \, \mathrm{sign}(h_{2,des} - h_2)$$

and K is derived from the second of Eqs. (21) as

$$K = (h^{\star}_{2,des} - H_0 \cos\Phi \sin\Theta)/(J_2 \dot{\Theta}_{des} \sin\Phi - J_2 \dot{\Psi}_{des} \cos\Phi \sin\Theta)$$

Note that K is set equal to zero when a negative value is obtained by the above procedure, which means that the wheel command forces angular momenta to track the current value of residual angular momentum along the body axes parallel to the active RWs, without accounting for precession and

nutation rate commands. This phase requires a relatively small amount of time, without jeopardizing convergence.

At the same time, an attenuation factor κ is introduced in Eq. (29), such that, as soon as this initial phase is completed (when present), the wheel torque command is driven slightly below saturation, thus recovering a residual sensitivity of the control law to precession and nutation rate commands, even when the saturation violation factor f is large. In this condition, the scaling factor simply makes desired angular rate time constants longer. Note that, as f approaches 1, k_{sat} becomes equal to K, with a smooth law. A value $\kappa = 0.1$ was selected as the best compromise between undesirable chattering, for κ close to 1, and large amplitude oscillations which cause convergence to require longer time intervals, for values of κ near zero.

Convergence is always reached, regardless of the value of κ. Nonetheless, when wide amplitude oscillations are present during the initial phase, convergence to the desired pointing attitude requires longer time. Conversely, when chattering occurs, the convergence remains fast, but, from the practical point of view, deformation degrees of freedom may be excited in the presence of flexible appendages, an effect which is not accounted for by the model adopted in the present study. This may cause overall maneuver performance degradation on a real spacecraft. The validity of the approach in handling saturation is demonstrated in the next Section by means of extensive sets of simulation runs for both deterministic initial conditions, in the case of rest-to-rest maneuvers, and randomly generated initial tumbling states.

4. Results

A dynamic model representative of a small satellite is considered for demonstrating the viability of the proposed control approach, as well as analyzing its convergence performance. A reference spacecraft is assumed, with an inertia tensor $\boldsymbol{J} = \text{diag}(10, 9, 8)$ kg m^2 and two identical active RWs, with moment of inertia $J_w = 0.001$ kg m^2. RWs are controlled by an electric motor torque with a time constant $\tau_h = 200$ ms and maximum torque $g_{max} = 50$ mN m. A residual angular momentum H_0 is present, with a nominal value of 0.850 N m s. Time constants $\tau_\Psi = \tau_\Theta = 2$ s are enforced for the desired precession and nutation angle responses, whereas a slower time constant $\tau_\Phi = 20$ s is assigned to the spin angle dynamics.

Numerical integration is performed by means of an explicit, 5$^{\text{th}}$ order accurate, variable, step Runge-Kutta algorithm. A maximum time-step of 50 ms is prescribed. Unless otherwise stated, a reference pointing problem is dealt with, for $\lambda = \pi/9$ rad and $\alpha = \pi/6$ rad. The error with respect to the desired pointing attitude is determined in terms of residual eigenaxis rotation amplitude, $\Delta\vartheta = 2\cos^{-1}\bar{q}_e$, where $\bar{q}_e$ is the scalar part of the quaternion error vector, $\boldsymbol{Q}_e = (\boldsymbol{q}_e^T, \bar{q}_e)^T$ [21]. The simulation is stopped at time t_f, when the residual error between current and desired quaternions falls below 0.017 rad = 0.1 deg, with a residual angular rate $\|\boldsymbol{\omega}_f\| < 0.0017$ rad/s = 0.01 deg/s. The effect of system parameters on maneuver time t_f is analyzed and discussed, with particular emphasis on the values of H_0 and g_{max}.

4.1. Rest-to-rest maneuvers

A rest-to-rest maneuver can be obtained if both initial and final attitudes are among admissible attitudes, with $\Theta_0 = \Theta(t = 0) = \pi/2$, and the residual angular momentum H_0 fully absorbed in the active RWs. This requires that, for a given value of λ, the initial pointing direction of the sensor, identified by its elevation α_0 and azimuth β_0 in $\mathcal{F}_I$, is such that $|\alpha_0| < \pi/2 - \lambda$. The initial equilibrium value of all system states can be determined, provided that at rest $\boldsymbol{\omega}_0 = (0, 0, 0)^T$, the initial value of quaternions is obtained from that of Euler angles, prescribed by Eq. (13), with $\Psi_0 = \Psi^\star + \beta_0$, $\Theta_0 = \pi/2$, and $\Phi_0 = \Phi^\star$, and the initial angular momentum stored in the active RWs is $h_{1_0} = H_0 \sin\Phi_0$ and $h_{2_0} = H_0 \cos\Phi_0$. Assuming that the final attitude is prescribed by the nominal pointing problem described above ($\lambda = \pi/9$, $\alpha = \pi/6$, and $\beta = 0$ for the considered choice of the frame of $\mathcal{F}_I$ described in subsection 2.2), a set of simulations is performed by sampling initial values of elevation and azimuth angles, α_0 and β_0, in order to determine the maneuver time t_f required for reaching the desired pointing attitude.

Figure 4 shows the contour plot for t_f as a function of α_0 and β_0 (Fig. 4.a) and a 3-D mesh plot of the resulting surface (Fig. 4.b). The point marked as T in Fig. 4.a represents the desired pointing direction. Convergence requires times ranging between 250 and almost 500 s for most of the feasible initial pointing attitudes. Figure 5 shows the time histories of spacecraft attitude variables (Figs. 5.a and b), and wheel torque and relative angular momenta (Fig. 5.c and d) when the initial pointing attitude is given by $\alpha_0 = -64$ deg and $\beta_0 = -105$ deg (point A in Fig. 4.a). The correct implementation of the proposed control strategy is clearly evident, where the precession angle

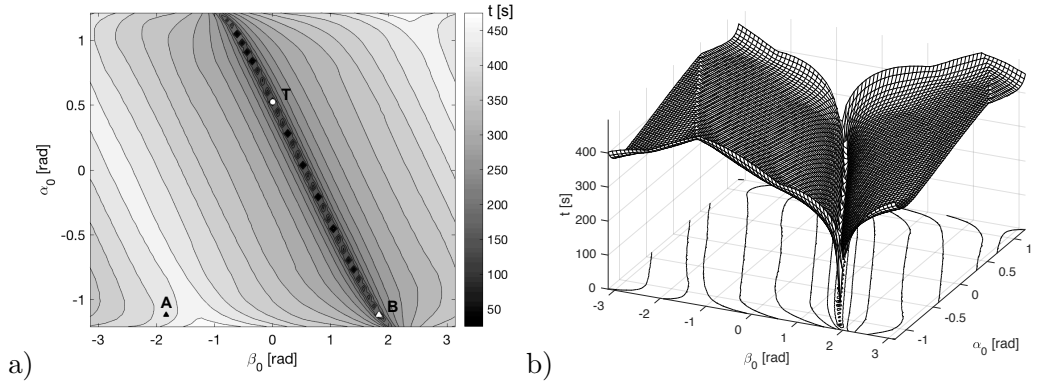

Figure 4: Contour (a) and mesh (b) plots for convergence time to target pointing condition T as a function of initial azimuth and elevation angles of sensor axis at rest.

reaches its prescribed value in little more than 50 s, and Θ is displaced up to the maximum admissible deviation for inducing a rotation around the spin axis, which exploits the residual angular momentum to drive Φ asymptotically towards its desired value. For the considered initial condition, a 180 deg variation of the (slowly varying) spin angle is required, which explains the long duration of the maneuver (438 s). The spikes visible in Fig. 5.c for the wheel control torques are induced by the various saturation levels present in the system (with the limit on the maximum RW torque) and in the control law (with a bound enforced on the maximum admissible nutation angle increment, ε_Θ). As a result of these saturation levels, wheel angular momentum command is only Lipschitz-continuous with respect to state variables, that is, it is continuous, with bounded discontinuities on its first derivatives, and sudden (but limited) variations in the torque required for tracking the resulting wheel angular velocity command are present. Nonetheless, the resulting variation of angular rates and wheel angular momenta are sufficiently smooth (Fig. 5.a and d, respectively).

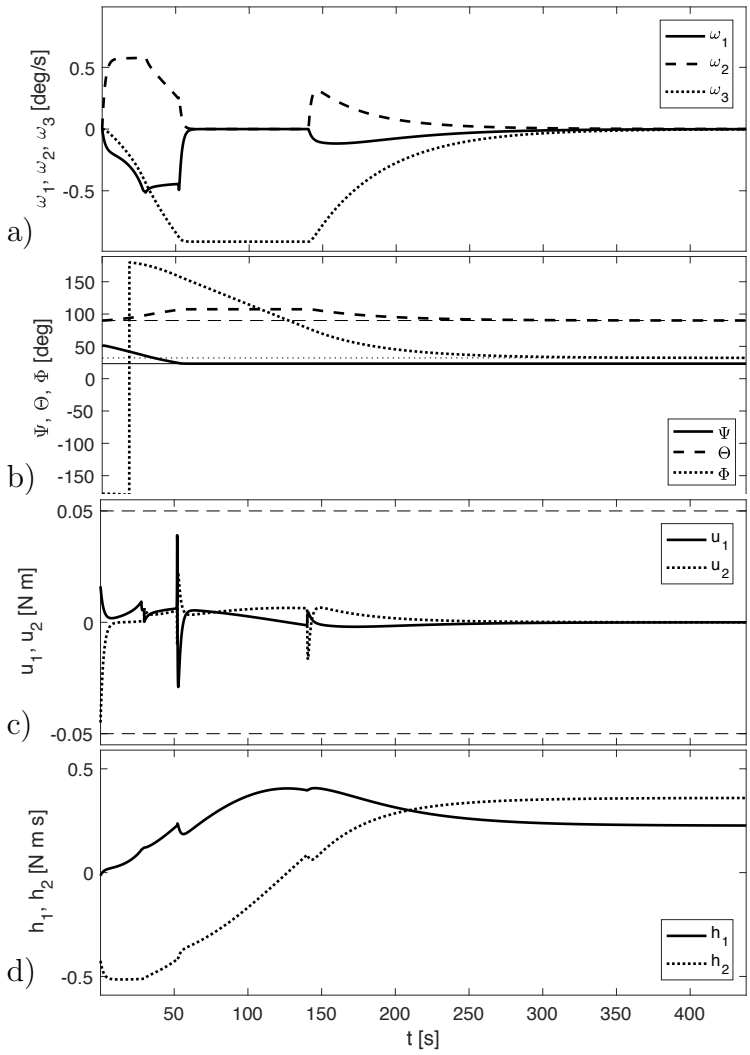

Figure 5: Simulation for initial condition A (black triangle in Fig. 4.a).

It is apparent that convergence time becomes significantly shorter if the initial pointing directions lies in the narrow "valley," clearly visible in the 3-D representation of t_f (Fig. 4.b), which includes the target attitude. Here, convergence time is below 250 s, being equal to less than 60 s along the bottom. The presence of this region of fast convergence is related to the values of Euler angles at initial time. All initial rest conditions require that

$\Theta_0 = \pi/2 \equiv \Phi_f$. If also $\Phi_0 \equiv \Phi_f$ for the considered values of α_0 and β_0, the desired pointing can be obtained by means of a simple single-axis rotation, which can be easily handled by the RWs. This is clearly visible in the time-histories of state and control variables shown in Fig. 6.a-d for the maneuver starting from the initial condition represented by the point labeled B in Fig. 4.a ($\alpha_0 = -64$ deg and $\beta_0 = 105$ deg). This point is the symmetric of A, with respect to the final desired attitude, being thus characterized by the same angular distante of $\hat{\boldsymbol{\sigma}}$ from its desired pointing direction, $\hat{\boldsymbol{\tau}}$, but it lies almost exactly at the bottom of the valley of fast maneuvers. Only two velocity components are varied during the maneuver (Fig. 6.a), in order to control the precession angle Ψ, whereas ω_3 remains close to 0 for its entire duration. Both Θ and Ψ remain almost exactly constant, at their initial values, Φ_0 being only 0.15 deg away from its final prescribed value. Note that,in cases with $\Phi_0 \approx \Phi_f$, the initial and final values of h_1 and h_2 are equal. Only 67 s are thus sufficient for reaching the prescribed pointing condition, which is approximately 7 times faster than the symmetric maneuver, starting from point A, which requires a 180 deg variation of the spin angle.

4.2. Monte Carlo simulations

Random initial conditions are generated in terms of both starting attitude and angular momentum distribution. More in detail, a random quaternion is generated, according to the technique proposed in [25]: given three uniformly distributed random numbers, $u, v, w \in [0, 1]$, the initial attitude quaternion is represented by $\boldsymbol{Q} = (\boldsymbol{q}_0^T, \bar{q})^T$, with

$$\boldsymbol{q}_0 = \left(\sqrt{1-u}\,\sin(2\pi v), \sqrt{1-u}\,\cos(2\pi v), \sqrt{u}\,\sin(2\pi w)\right)^T \;,\; \bar{q}_0 = \sqrt{u}\,\cos(2\pi w)$$

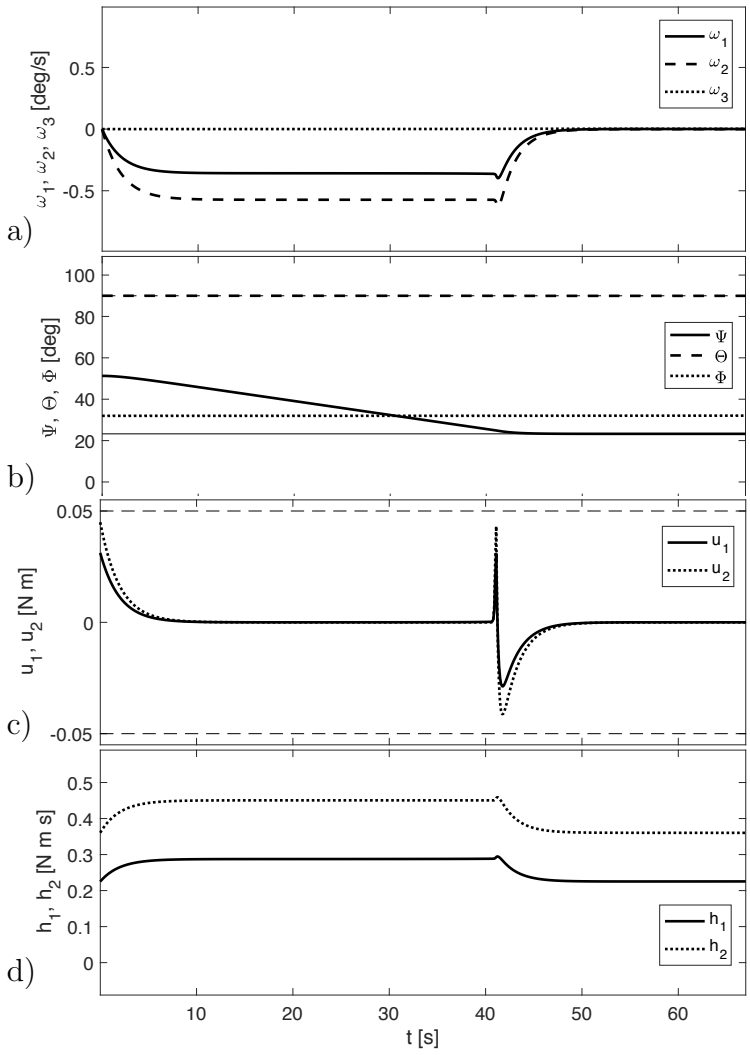

Figure 6: Simulation for initial condition B (white triangle in Fig. 4.a).

The initial angular momentum of each wheel is also assumed as a bounded random variable, with $h_{i,0} = (2\sigma_i - 1)H_0$, $i = 1, 2$, where $\sigma_i \in [0, 1]$, $i = 1, 2$ are two uniformly distributed random variables. The resulting initial value for angular rates is thus given by $\boldsymbol{\omega}_0 = \boldsymbol{J}^{-1}\left[\mathbb{T}_{BI}(\boldsymbol{q}_0, \bar{q}_0)(0, 0, H_0)^T - \boldsymbol{h}\right]$, with $h_{i,0} \in [-H_0, H_0]$.

An initial set of 10,000 simulations is run for the nominal values of residual

angular momentum, $H_0 = 0.850$ N m s, and wheel torque saturation levels, $g_{max} = 50$ mN m. Four more Monte Carlo simulation campaigns are then performed, each one made of 10,000 randomly generated initial conditions, for evaluating the effects of residual angular momentum and maximum wheel torque on convergence performance, t_f. H_0 is varied by $\pm 50\%$ first, generating two cases for $H_0 = 0.425$ N m s and $H_0 = 1.275$ N m s, respectively, with $g_{max} = 50$ mN m. Similarly, the wheel motor saturation torque is varied by $\pm 50\%$, generating two more cases for $g_{max} = 25$ mN m and 75 mN m, with $H_0 = 0.850$ N m s.

Table 1 lists the results of the five Monte Carlo tests (the nominal case is repeated twice for the sake of readability), in terms of average value of convergence time, $\bar{t}_f$, over the whole set of tests, its standard deviation, $\sigma(t_f)$, and three relevant percentiles (10%, 50%, and 90%). The corresponding probability density functions (PDFs) for convergence time t_f are presented in Figs. 7 and 8. Note that in these plots the abscissa is reported in terms of hundreds of seconds, so that each PDF achieves values in the order of 1.

It is apparent from the results of the first set of Monte Carlo simulations, where H_0 is varied, that the effect of the residual angular momentum on convergence performance is relatively modest, when random initial conditions are considered. Only when H_0 is decreased, a slightly longer average convergence time is obtained (approximately 7% longer than the nominal case), with a slightly wider dispersion (standard deviation increases by 11%). This is due to a longer time required for the final convergence of the spin angle, which becomes slower, when a reduced value of H_0 is available. Conversely, the probability density functions for an increased value of H_0 is almost ex-

Table 1: Results from Monte Carlo simulations

Case	**Variation of H_0**				
	avg.	std.dev.	Percentiles		
	$\bar{t}_f$	$\sigma(t_f)$	0.1	0.5	0.9
-50%	298	75.9	198	299	395
nominal	262	68.4	178	257	358
+50%	264	74.2	172	257	368
Case	**Variation of g_{max}**				
	avg.	std.dev.	Percentiles		
	$\bar{t}_f$	$\sigma(t_f)$	0.1	0.5	0.9
-50%	438	151.3	236	434	646
nominal	262	68.4	178	257	358
+50%	210	49.4	148	207	278

actly equal to that of the nominal case.

As expected, the variations of wheel torque saturation level result into more significant variations of both average convergence time and standard deviation, where an increase by 50% of wheel saturation torque allows for reducing convergence time by 20%, on average, with a narrower distribution, $\sigma(t_f)$ being reduced by almost 28%. On the other hand, when maximum wheel torque is reduced by 50%, $\bar{t}_f$ increases by 67%, and $\sigma(t_f)$ becomes more than double. The probability density function, in this latter case, looses its peak and becomes almost constant, over a wide interval.

The correlation between convergence time and initial pointing error $\Delta\vartheta$ is analyzed in Figs. 9 and 10, where the three subplots in Fig. 9 are obtained for

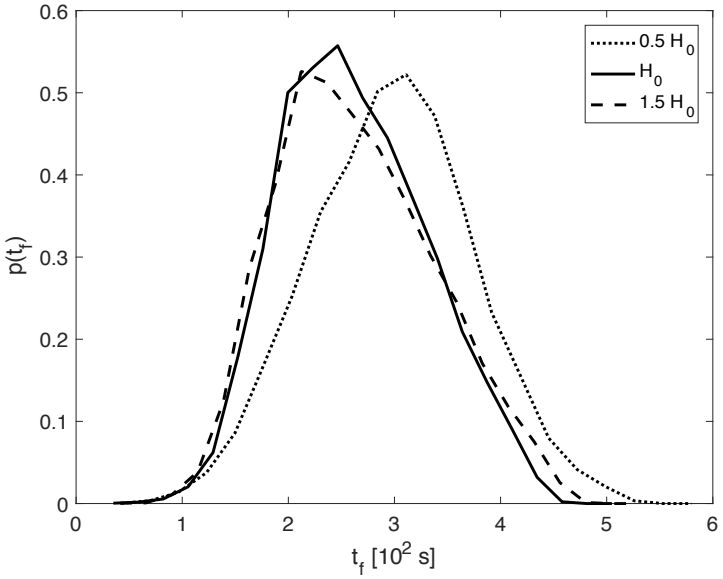

Figure 7: Probability density functions for different values of H_0.

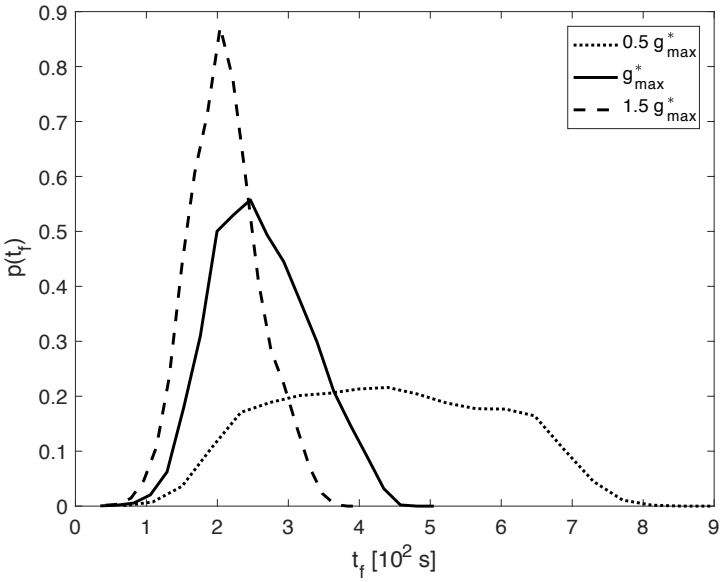

Figure 8: Probability density functions for different values of g_{max}.

the nominal value of g_{max} and different values of H_0, whereas Fig. 10 shows the results for three values of g_{max} and nominal H_0. Each run is represented by a grey point on the $\Delta\vartheta$ vs t_f plane. The plots also reports the trend of the

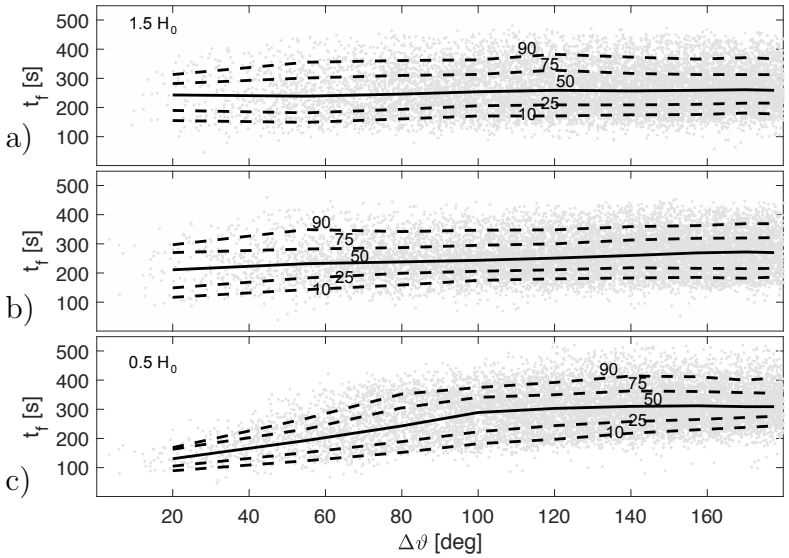

Figure 9: Plot of t_f vs $\Delta\vartheta$ for various H_0.

percentiles, with the 50$^{\text{th}}$ percentile represented by a continuous black line. When H_0 is higher, the distribution of convergence time is almost unaffected by $\Delta\vartheta$ (Fig. 9.a), with almost exactly horizontal percentiles lines. A slight increase of t_f with $\Delta\vartheta$ is apparent for the nominal value of H_0, although quite limited (Fig. 9.b), whereas the third plot (Fig. 9.c), traced for a reduced value of the residual angular momentum, reports a more visible trend with wider dispersion, but also a more significant increase of convergence time as a function of the initial pointing error.

When the effect of g_{max} is considered (Fig. 10), the increase in the percentile lines with $\Delta\vartheta$ is limited, over the whole range of initial pointing errors. For the highest saturation torque considered (Fig. 10.a), the 50$^{\text{th}}$ percentile grows from 160 s, for initial pointing error in the range between 0 and 40 deg, up to 210 s, when the initial error exceeds 170 deg. , The same indicator grows from 210 s up to 270 s if the nominal value of g_{max} is considered

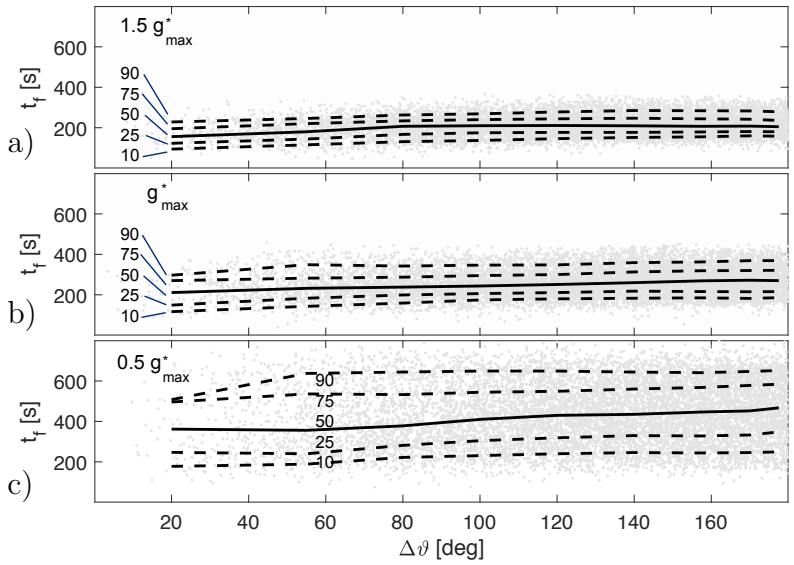

Figure 10: Plot of t_f vs $\Delta\vartheta$ for various g_{max}.

(Fig. 10.b) as $\Delta\vartheta$ is larger, whereas longer convergence times are required for 50% of the sample population, when $g_{\max}$ is halved (Fig. 10.c), with convergence time as large as 360 s for smaller initial errors, up to almost 470 s. The other percentile lines follow a similar pattern, such that dispersion remains almost constant, thus getting broader, for smaller values of the wheel motor saturation torque, as already pointed out from the analysis of the resulting global PDF.

Figure 11 reports the time histories for the worst case scenario obtained in the framework of the Monte Carlo simulation of 10,000 runs for nominal system parameters, that is, the maneuver requiring the longest convergence time, equal to $t_f = 467$ s. Figure 11.a, where the variation of angular velocity components is presented, shows that the initial tumbling motion for the randomly generated initial condition is relatively high, so that the initial portion of the maneuver is used to rapidly slow down the angular velocity,

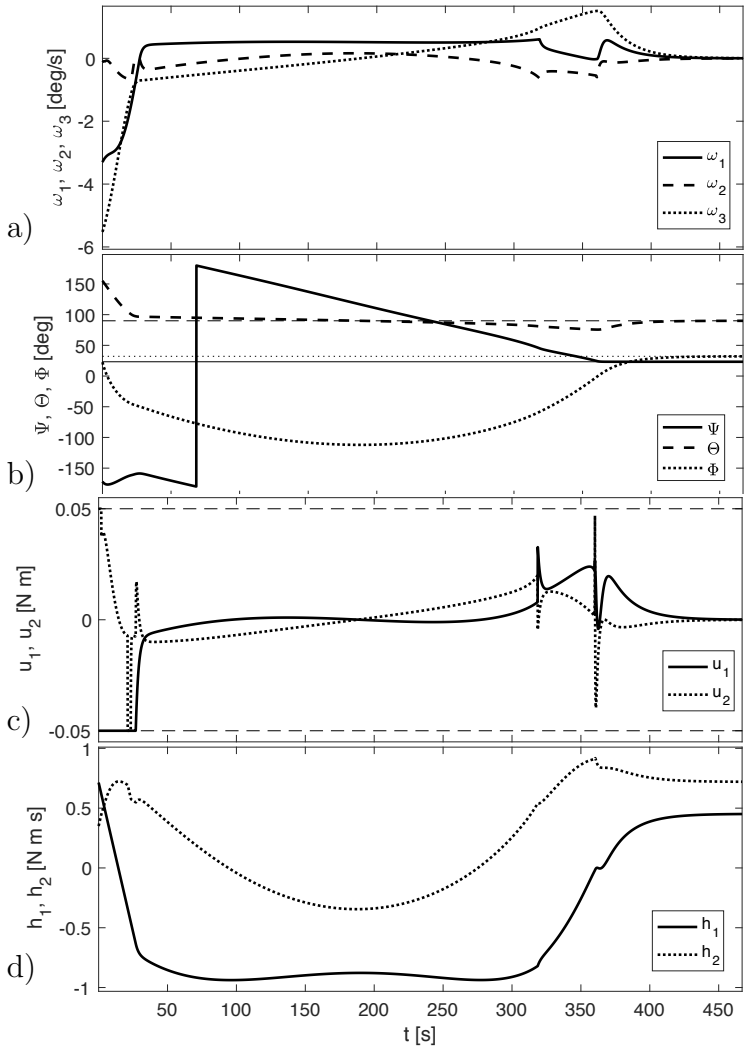

Figure 11: Worst case in Monte Carlo simulation for nominal system parameters.

with Θ being drawn close to its desired value, $\Theta_f = 90$ deg. This is done by saturating the control torque on one of the wheels (as shown in Fig. 11.c). This fast initial transient, during which the error on precession and nutation angles is uncontrolled, is required for reducing the RWs angular momenta to the point where the desired commands can be implemented. After this

initial phase, the precession angle error decreases linearly until, during the final phase, also the spin angle asymptotically reaches its desired value, on a slower timescale.

The spikes in the control torque, visible in Fg. 11.c, are caused by the discontinuities on the time derivative of $h_{1,des}$ and $h_{2,des}$ induced by the method adopted for managing saturation, as discussed in subsection 3.4. When control torque demand from the baseline controller exceeds saturation limits, the saturation factor f and the scaling factor for the control law, k_{sat}, are determined from the value of the torque required by the wheel, which violates the saturation constraint more severely. When this condition switches from one active wheel to the other one, or when saturation is no longer violated, a discontinuity on the derivative of both $h_{1,des}$ and $h_{2,des}$ is present, which induces a step variation on the resulting control torque, rapidly compensated. Note that the variation of wheel angular momenta remains smooth (Fg. 11.d).

4.3. Convergence towards the bounds of the region of admissible pointing directions

Performance for pointing at the boundary of the admissible pointing region, where $\alpha = \alpha_{max} = \pi/2 - \lambda$ is finally considered. As outlined in subection 2.4, all desired values of Euler angles are equal to 90 deg, in this case, and the whole residual angular momentum is absorbed by only one of the wheels, at convergence.

Figure 12 shows the time histories of attitude (Fig. 12.a and b) and control (Fig. 12.c and d) variables for nominal torque saturation and residual angular momentum, for a randomly generated set of initial conditions. It is apparent that convergence follows a pattern similar to that observed in

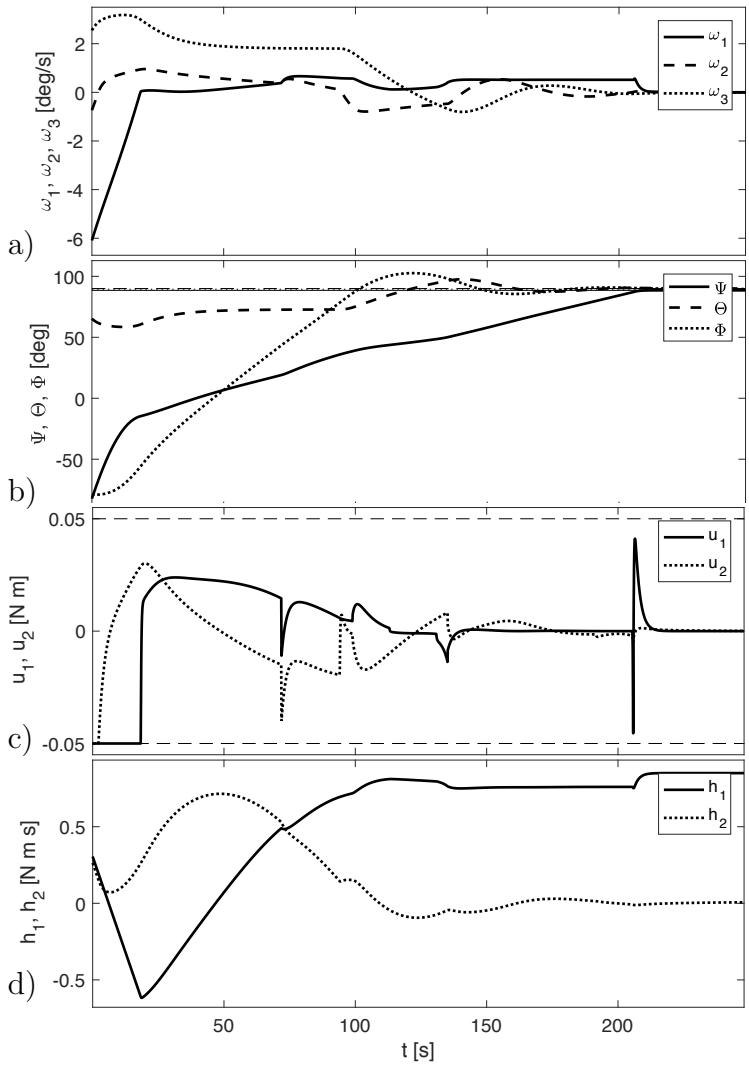

Figure 12: Simulation of convergence to the bound of the admissible pointing region for nominal system parameters and randomly generated initial conditions.

previous simulations (including a few spikes in the control torque). The only relevant difference, exhibited also by other simulations not reported for the sake of conciseness, is that the spin angle Φ often converges towards its desired value faster than the precession angle, Ψ. As for the remaining features

of time-histories, there is no other relevant observation: angular rates are reduced first, while Θ approaches 90 deg, with a rather smooth variation of all attitude variables.

5. Conclusion

The possibility of aiming a generic body–fixed axis towards a prescribed direction in space when only two reaction wheels are available for attitude control of a rigid spacecraft was discussed, in the presence of a residual angular momentum, while driving the spacecraft at rest. First of all, a feasibility condition for the pointing maneuver was derived, proving that a fixed direction in space can be reached only in those cases when its angular separation from the direction of the inertially fixed angular momentum vector is smaller than the angular separation between the body–fixed axis and the axis of the failed reaction wheel. Moreover, the values of the precession, nutation and spin angles that allow for the desired pointing were analytically derived, showing that the nutation angle must be equal to $\pi/2$ if spacecraft angular rate needs to be driven to zero.

A control law, based on the timescale separation principle, is proposed, where different timescales for active wheel angular momenta and desired Euler angle dynamics are enforced by a careful selection of the control law gains. In the presence of saturation, these gains are modified, in order to maintain the timescale separation. The resulting behavior under the action of the proposed control law, analyzed for rest-to-rest maneuvers and for initial randomly generated tumbling conditions, demonstrates the viability of the approach over a wide number of test cases.

Appendix

Remembering that $\Theta_f = \pi/2$, so that $\sin\Theta = \sin(\Theta_f + e_\Theta) = \cos e_\Theta$, Eqs. (17), (18), and (22) can be recast in error form,

$$\dot{e}_\Psi = -\frac{1}{\tau_\Psi} e_\Psi - \frac{\sin\Phi}{\cos e_\Theta}\frac{e_{h1}}{J_1} - \frac{\cos\Phi}{\cos e_\Theta}\frac{e_{h2}}{J_2} \tag{30}$$

$$\dot{e}_\Theta = -\frac{1}{\tau_\Theta} e_\Theta - \cos\Phi\frac{e_{h1}}{J_1} + \sin\Phi\frac{e_{h2}}{J_2} \tag{31}$$

$$\varepsilon\dot{e}_{h,i} = -e_{h,i} - \varepsilon\dot{h}_{i,des}\ , \quad i = 1,2 \tag{32}$$

with $\varepsilon = \tau_h$. The complete expressions of $\dot{h}_{1,des}$ and $\dot{h}_{2,des}$ derived from Eqs. (21), and accounting for Eqs. (20), are not reported for the sake of conciseness. A more compact version is obtained for $\tau_\Psi = \tau_\Theta = T_s$, such that

$$\begin{aligned}
\dot{h}_{1,des} = &-(H_0^2/J_3)\sin e_\Theta\cos e_\Theta\cos\Phi - (1 - e_\Theta\tan e_\Theta\sin^2\Phi)e_{h1}/T_s \\
&+ [(J_1/J_2)(e_\Theta\cos\Phi\sin\Phi/\cos e_\Theta - e_\Psi)(1/T_s) - H_0/J_2]\sin e_\Theta e_{h2} \\
&+ [H_0(1 + J_1/J_3)\sin\Phi\sin e_\Theta + J_1(2e_\Psi\sin e_\Theta\sin\Phi - \cos\Phi)(1/T_s)]e_\Theta/T_s \\
&- [H_0(1 + J_1/J_3)\cos\Phi\sin e_\Theta\cos e_\Theta \\
&\qquad + J_1(\sin\Phi + e_\Psi\cos\Phi\sin e_\Theta)(1/T_s)\cos e_\Theta]e_\Psi/T_s \\
\dot{h}_{2,des} = &\ (H_0^2/J_3)\sin\Phi\sin e_\Theta\cos e_\Theta \\
&+ [H_0/J_1 + (J_2/J_1)(e_\Psi + e_\Theta\cos\Phi\sin\Phi/\cos e_\Theta)(1/T_s)]\sin e_\Theta e_{h1} \\
&- (1 - e_\Theta\tan e_\Theta\cos^2\Phi)e_{h2}/T_s \\
&+ [H_0\cos\Phi\sin e_\Theta(1 + J_2/J_3) + J_2(\sin\Phi + 2e_\Psi\cos\Phi\sin e_\Theta)(1/T_s)]e_\Theta/T_s \\
&+ [H_0(1 + J_2/J_3)\sin\Phi\sin e_\Theta\cos e_\Theta \\
&\qquad + J_2(e_\Psi\sin\Phi\sin e_\Theta - \cos\Phi)\cos e_\Theta(1/T_s)]e_\Psi/T_s
\end{aligned}$$

After the initial transient, when Θ becomes sufficiently close to $\Theta_f = \pi/2$ (hence $\cos e_\Theta \approx 1$), all terms in the expressions of $\dot{h}_{1,des}$ and $\dot{h}_{2,des}$ are proportional to

the inverse of either one of the slow timescales, namely τ_Θ, τ_Ψ, or J_i/H_0, such that the terms $\varepsilon\dot{h}_{i,des}$ in Eqs. (32), for $i = 1, 2$, are vanishing with respect to the perturbation parameter ε. This result is not surprising, if one considers that $h_{1,des}$ and $h_{2,des}$ depend on slow variables only, hence $h_{i,des}$ can be considered (almost) constant on the fast time scale, so that $\dot{h}_{i,des} \approx 0$.

If error dynamics is recast in a standard singular perturbation form,

$$\begin{aligned} \dot{\boldsymbol{\xi}} &= \boldsymbol{F}(\boldsymbol{\xi}, \boldsymbol{\zeta}, t, \varepsilon) \\ \varepsilon\dot{\boldsymbol{\zeta}} &= \boldsymbol{G}(\boldsymbol{\xi}, \boldsymbol{\zeta}, t, \varepsilon) \end{aligned}$$

with $\boldsymbol{\zeta} = (e_{h1}, e_{h2})^T$, $\boldsymbol{\xi} = (e_\Psi, e_\Theta)^T$, and $\varepsilon = \tau_h \ll T$, all of the 5 assumptions for Theorem 11.4 of Ref. [24] apply to the present system. In detail

1. $\boldsymbol{F}(0, 0, t, \varepsilon) = 0$ and $\boldsymbol{G}(0, 0, t, \varepsilon) = 0$;
2. the equation $\boldsymbol{G}(\boldsymbol{\xi}, \boldsymbol{\zeta}, t, 0) = 0$ has an isolated root, $\boldsymbol{\zeta} = \boldsymbol{h}(t, \boldsymbol{x})$, such that $\boldsymbol{h}(t, 0) = 0$; in the present case the isolated root is simply $e_{h1} = e_{h2} = 0$;
3. the functions $\boldsymbol{F}$, $\boldsymbol{G}$ and $\boldsymbol{h}$ and their partial derivatives up to second order are bounded, which is true, in the neighborhood of $\Theta \approx \Theta_f = \pi/2$;
4. the origin of the reduced system $\dot{\boldsymbol{\xi}} = \boldsymbol{F}(\boldsymbol{\xi}, \boldsymbol{h}(t, \boldsymbol{\xi}), t, 0)$ is exponentially stable;
5. letting $\boldsymbol{\eta} = \boldsymbol{\zeta} - \boldsymbol{h}(\boldsymbol{\xi}, t)$, the origin of the boundary-layer system $\dot{\boldsymbol{\eta}} = \boldsymbol{G}(\boldsymbol{\xi}, \boldsymbol{\eta} + \boldsymbol{h}(t, \boldsymbol{\xi}), t, 0)$ is exponentially stable.

The latter two conditions are clearly satisfied by the considered system. Hence, the origin of the system written in terms of error dynamics is (locally) exponentially stable, if ε is sufficiently small.

References

[1] B. Wie, P. M. Barba, Quaternion feedback for spacecraft large angle maneuvers, Journal of Guidance, Control, and Dynamics 8 (3) (1985) 360–365. doi:10.2514/3.19988.

[2] E. L. De Angelis, F. Giulietti, de Ruiter Anton H.J., G. Avanzini, Spacecraft attitude control using magnetic and mechanical actuation, Journal of Guidance, Control, and Dynamics 39 (3) (2016) 564–573. doi:10.2514/1.G000957.

[3] A. Zavoli, G. De Matteis, F. Giulietti, G. Avanzini, Single-axis pointing of an underactuated spacecraft equipped with two reaction wheels, Journal of Guidance, Control, and Dynamics 40 (6) (2017) 1465–1471. doi:10.2514/1.g002182.

[4] G. Avanzini, F. Giulietti, Constrained slews for single-axis pointing, Journal of Guidance, Control, and Dynamics 31 (6) (2008) 1814–1817. doi:10.2514/1.38291.

[5] E. L. De Angelis, F. Giulietti, G. Avanzini, Single-axis pointing of underactuated spacecraft in the presence of path constraints, Journal of Guidance, Control, and Dynamics 38 (1) (2015) 143–147. doi:10.2514/1.G000121.

[6] N. M. Horri, P. Palmer, Practical implementation of attitude-control algorithms for an underactuated satellite, Journal of Guidance, Control, and Dynamics 35 (1) (2012) 40–45. doi:10.2514/1.54075.

[7] P. C. Hughes, Spacecraft attitude dynamics, Dover Publications, Mineola, N.Y., 2004.

[8] J. R. Wertz, Spacecraft Attitude Determination and Control, Springer, 1978.

[9] A. Zavoli, F. Giulietti, G. Avanzini, G. D. Matteis, Spacecraft dynamics under the action of y-dot magnetic control law, Acta Astronautica 122 (2016) 146–158. doi:10.1016/j.actaastro.2016.01.024.

[10] P. Tsiotras, V. Doumtchenko, Control of spacecraft subject to actuator failures: State-of-the-art and open problems, in: Proceedings of the R.H. Battin Astrodynamics Symposium, College Station, TX, March 20-21, 2000, 2000, pp. AAS Paper 00–264.

[11] P. Tsiotras, J. M. Longuski, Spin-axis stabilization of symmetric spacecraft with two control torques, Systems & Control Letters 23 (6) (1994) 395–402.

[12] S. Kim, Y. Kim, Spin-axis stabilization of a rigid spacecraft using two reaction wheels, Journal of Guidance, Control, and Dynamics 24 (5) (2001) 1046–1049. doi:10.2514/2.4818.

[13] K. Yamada, N. Takatsuka, T. Shima, Spacecraft pointing control using a variable-speed control moment gyro, Transactions of the Japan Society for Aeronautical and Space Science, Space Technology Japan 7 (ists26) (2009) 1–6.

[14] P. Tsiotras, M. Corless, M. Longuski, A novel approach to the attitude control of axisymmetric spacecraft, Automatica 31 (8) (1995) 1099–1112.

[15] J. Jin, Attitude control of underactuated and momentum-biased satellite using state-dependent riccati equation method, International Journal of Aeronautical and Space Sciences 20 (1) (2018) 204–213. doi:10.1007/s42405-018-0104-5.

[16] A. Golzari, H. N. Pishkenari, H. Salarieh, T. Abdollahi, Quaternion based linear time-varying model predictive attitude control for satellites with two reaction wheels, Aerospace Science and Technology 98 (2020) 1–10. doi:10.1016/j.ast.2019.105677.

[17] C. Yue, F. Wu, F. Wang, X. Cao, Q. Shen, K. D. Kumar, Two parallel single-gimbal control moment gyros actuated spacecraft attitude maneuver, IEEE Transactions on Aerospace and Electronic Systems 56 (5) (2020) 4112–4123. doi:10.1109/taes.2020.2974053.

[18] H. Yoon, P. Tsiotras, Spacecraft line-of-sight control using a single variable-speed control moment gyro, Journal of Guidance, Control, and Dynamics 29 (6) (2006) 1295–1308. doi:10.2514/1.18777.

[19] S. Kwon, T. Shimomura, H. Okubo, Pointing control of spacecraft using two SGCMGs via LPV control theory, Acta Astronautica 68 (7-8) (2011) 1168–1175. doi:10.1016/j.actaastro.2010.10.001.

[20] P. V. Kokotović, Application of singular perturbation techniques to control problems, SIAM Review 26 (4) (1984) 501–550.

[21] B. Wie, Space vehicle dynamics and control, AIAA Ed. Series, 1998.

[22] R. F. Stengel, Optimal Control and Estimation, Dover Publications, Mineola, N.Y., 1994.

[23] W. M. Haddad, V. Chellaboina, Nonlinear dynamical systems and control: a Lyapunov-based approach, Princeton University Press, 2008.

[24] H. K. Khalil, J. Grizzle, Nonlinear systems, Prentice Hall, 2002.

[25] K. Shoemake, Uniform random rotations, in: D. Kirk (Ed.), Graphics Gems III, Academic Press, New York, 1992, pp. 124–132.